Electronic Supplementary Material (ESI) for Dalton Transactions.
This journal is © The Royal Society of Chemistry 2022

BODIPY-dipicolylamine complexes of platinum(II): X-ray structure, cellular imaging and organelles specific near-IR light type-II PDT

Arpan Bera,[a] Srishti Gautam,[b] Md Kausar Raza,[a] Apurba Kumar Pal,[a] Paturu Kondaiah,[*b] and Akhil R. Chakravarty[*a]

[a] *Department of Inorganic and Physical Chemistry, Indian Institute of Science, Sir C.V. Raman Avenue, Bangalore 560012, India. E-mail: arc@iisc.ac.in*

[b] *Department of Molecular Reproduction, Development and Genetics, Indian Institute of Science, Bangalore 560012, India. E-mail: paturu@iisc.ac.in*

Electronic Supplementary Information (ESI)

Table of contents

Figure S17. (a) Absorption and (b) emission spectra of ligand $\mathbf{L^2}$ in 1:1 (v/v) DMSO/DPBS. (c) Absorption and (d) emission spectra of ligand $\mathbf{L^3}$ in 1:1 (v/v) DMSO/DPBS.

Figure S18. Fluorescence quantum yield for $\mathbf{L^3}$ in DMF.

Figure S19. Fluorescence quantum yield for complex **2** in DMF.

Figure S20. Fluorescence quantum yield for complex **3** in DMF.

Figure S21. Lifetime decay profile for lifetime measurement of complex **2** in DMF.

Figure S22. (a) ORTEP diagram of two molecules of complex **2a** in the crystallographic asymmetric unit. One perchlorate anion oxygen atom positional disorder is shown. Colour codes used: platinum, red; carbon, black; nitrogen, blue; boron, ivory; fluorine, light green; chlorine, deep green. (b) Unit cell packing diagram showing the presence of solvent of crystallization. (c, d) view of disordered perchlorate along O11-C11, C_3 axis.

Figure S23. (a) Optimized structure and (b) nodal patterns of HOMO and LUMO of complex **2** as generated over optimized structure.

Figure S24. (a) Optimized structure and (b) nodal patterns HOMO and LUMO of complex **3** as generated over optimized structure.

Figure S25. Time-dependent stability studies of complex **2** in 1:1 (v/v) DMSO/DPBS under dark condition.

Figure S26. Time-dependent stability studies of complex **3** in 1:1 (v/v) DMSO/DPBS under dark condition.

Figure S27. Time-dependent stability studies of complex **1** in 10% DMSO/DMEM under dark condition.

Figure S28. Time-dependent stability studies of complex **2** in 10% DMSO/DMEM under dark condition.

Figure S29. Time-dependent stability studies of complex **3** in 10% DMSO/DMEM under dark condition.

Figure S30. Time-dependent stability studies of complex **1** in presence of 10 eqv. GSH under dark condition.

Figure S31. Time-dependent stability studies of complex **2** in presence of 10 eqv. GSH under dark condition.

Figure S32. Time-dependent stability studies of complex **3** in presence of 10 eqv. GSH under dark condition.

Figure S33. Time-dependent stability studies by ^{1}H NMR of complex **1** in DMSO-d_6-DPBS mixture under dark condition.

Figure S34. Time-dependent stability studies by ^{1}H NMR of complex **2** in DMSO-d_6-DPBS mixture under dark condition.

Figure S35. Time-dependent stability studies by ^{1}H NMR of complex **3** in DMSO-d_6-DPBS mixture under dark condition.

Figure S36. Photostability studies of complex **1** in 10 % DMSO/DPBS (dose: 10 J/cm^2, 400-700 nm wavelength).

Figure S37. Photostability studies of complex by ^{1}H NMR **1** in DMSO-d_6-DPBS mixture (dose: 10 J/cm^2, 400-700 nm wavelength).

Figure S38. Photostability studies of complex **2** in 10 % DMSO/DPBS (dose: 10 J/cm^2, 400-700 nm wavelength).

Figure S39. Photostability studies of complex **2** by ^{1}H NMR in DMSO-d_6-DPBS mixture (dose: 10 J/cm^2, 400-700 nm wavelength).

Figure S40. Photostability studies of complex **3** in 10 % DMSO/DPBS (dose: 30 J/cm^2, 600-720 nm wavelength).

Figure S41. Photostability studies of complex **3** in by ^{1}H NMR DMSO-d_6-DPBS mixture (dose: 30 J/cm^2, 600-720 nm wavelength).

Figure S42. Cell viability plots obtained from MTT assay of complex **1** in HeLa cells under light (400-700 nm, 1 h exposure, light dose: 10 J cm^{-2}) and dark condition.

Figure S43. Cell viability plots obtained from MTT assay of complex **1** in A549 cell line under light (400-700 nm, 1 h exposure, light dose: 10 J cm^{-2}) and dark condition.

Figure S44. Cell viability plots obtained from MTT assay of complex **2** in HeLa cell line under light (400-700 nm, 1 h exposure, light dose: 10 J cm^{-2}) and dark condition.

Figure S45. Cell viability plots obtained from MTT assay of complex **2** in A549 cell line under light (400-700 nm, 1 h exposure, light dose: 10 J cm^{-2}) and dark condition.

Figure S46. Cell viability plots obtained from MTT assay of complex **3** in HeLa cell line under light (600-720 nm, 20 min exposure, light dose: 30 J cm^{-2}) and dark condition.

Figure S47.viability plots obtained from MTT assay of complex **3** in A549 cell line under light (600-720 nm, 20 min exposure, light dose: 30 J cm^{-2}) and dark condition.

Figure S48. Cell viability plots obtained from MTT assay of complex **1** in HPL1D cells under light (400-700 nm, 1 h exposure, light dose: 10 J cm^{-2}) and dark condition.

Figure S49. Cell viability plots obtained from MTT assay of complex **2** in HPL1D cells under light (400-700 nm, 1 h exposure, light dose: 10 J cm^{-2}) and dark condition.

Figure S50. Cell viability plots obtained from MTT assay of complex **3** in HPL1D cells under light (400-700 nm, 1 h exposure, light dose: 10 J cm^{-2}) and dark condition.

Figure S51. Changes in absorption spectra of DBBF containing complex **2** (50:1 concentration ratio) under visible light (400-700 nm, 10 J cm^{-2}) in DMSO.

Figure S52. ΔOD vs. irradiation time for determining singlet oxygen quantum yield of complex **2**.

Figure S53. Confocal images for A549 cells with suitable trackers and complex 3. Panels (i) and (v) show blue emission of nucleus staining dye DAPI, panels (ii) and (vi) show green emission of trackers (iii) and (vii) show red emission of complex 3 and panels (iv) and (viii) show merged images.

Figure S54. Standard plot for ICP-MS study for Pt content determination.

Figure S55. Dot plot of annexin V-FITC/PI data of (a) cells only, (b) cells + annexin, (c) cells + PI, (d) cells + annexin +PI, (e) cells + complex **1** (in light, λ =600-720 nm, 30 J cm^{-2}, 20 min irradiation) and (f) cells + complex **1** (in dark) in A549 cell line.

Figure S56. Cell cycle progression of complex **1** under light and dark condition using A549 cancer cell line.

Figure S57. binding plot for complex **2** in presence of 10 % DMF-Tris-HCl buffer (pH = 7.2) and ct-DNA at 25 °C. (a) changes in absorption spectra with each addition of ct-DNA and (b) McGhee-von Hippel (MvH) plot [DNA]/(ε_f - ε_a) vs. [DNA].

Figure S58. DNA binding plot for complex **3** in presence of 10 % DMF-Tris-HCl buffer (pH = 7.2) and ct-DNA at 25 °C. a) changes in absorption spectra with each addition of ct-DNA and (b) McGhee-von Hippel (MvH) plot [DNA]/(ε_f - ε_a) vs. [DNA].

Table S1. Selected crystallographic parameters for complex **2a**

Table S2. Selected bonding parameters, namely, bond lengths (Å) and bond angles (°) for complex **2a**

Table S3. Coordinates of optimized geometry for complex **1** obtained from DFT using B3LYP/LanL2DZ level of theory for all atoms

Table S4. Coordinates of optimized geometry for complex **2** obtained from DFT using B3LYP/LanL2DZ level of theory for all atoms

Table S5. Coordinates of optimized geometry for complex **3** obtained from DFT using B3LYP/LanL2DZ level of theory for all atoms

Table S6. Comparison of IC_{50} (μM) values of complexes **1-3** with recently reported platinum(II)-anticancer complexes

Experimental section

Crystallography and theoretical methods: Complex **2a**, as a perchlorate salt of complex **2**, having green light BODIPY was characterized by single-crystal X-ray crystallographic method. Complex **2a** was crystallized as orange coloured needle shaped crystals that were obtained from acetonitrile solution on slow evaporation. A crystal of 0.22 × 0.16 × 0.12 mm^3 size was mounted on a loop with mineral oil. All intensity and geometrical data were collected by using an automated Bruker SMART APEX CCD diffractometer. Instrument is equipped with a 1.75 kW sealed-tube Molybdenum K_α X-ray source of wavelength 0.71073 Å having an increasing ω and width is 0.3° per frame. Data were collected in 5 sec per frame scan speed. Scan mode ω-2θ was used for intensity data collection. Lorentz-polarization and absorption corrections were taken into consideration.[S1] WinGX software of the version 1.63.04a was used to solve the structure and ShelXL-2018/3 method was employed.[S2] Refinement of non-hydrogen atoms were performed using anisotropic displacement coefficients and their corresponding coordinates were allowed to ride on their respective non-hydrogen atoms. The solvent water molecules in the crystals being highly disordered necessitated the use of SQUEEZE option of PLATON suite software to remove the scattering from highly disordered solvent molecules (vide ESI† for details). The final refinement includes anisotropic thermal parameter of the non-hydrogen atoms, all atom positions, the isotropic thermal parameters of all the hydrogen atoms. By using ORTEP, perspective views were obtained.[S3]The CCDC

deposition number of complex **2a** is 2083988. Theoretical studies were made using density functional theory (DFT) to obtain the energy minimized structures and nodal patterns of frontier molecular orbitals (FMO) on optimized geometry.[S4] All the structures were optimized using Gaussian09 suite of programmes with B3LYP (Becke,3-parameter, Lee-Yang-Parr hybrid functional) level of theory and LanL2DZ basis set.[S5,S6]

ICP-MS: Around 10^5 A549 cells were seeded in 90 mm tissue culture dishes to measure whole cell platinum uptake. Cells were pretreated with complexes **2** and **3** (5 μM) and kept for 4 h incubation. Medium was removed and DPBS buffer was added. 300 µL of 70 % HNO_3 was used for cell lysate. Lysate was transferred to 15 mL tubes. Tubes were allowed to stand at room temperature for 15 mins. 100 µL H_2O_2 was added to lysate and incubated for 3 h at 55 °C. After that lysate was diluted to 10 mL and subjected to ICP-MS analysis to determine platinum content. Experiment was run along with the standards (0.01-1.0 ppm), and a blank sample fitted in a linear plot with a correlation of 0.99. Platinum content obtained in ppb units was then expressed as ng of Pt/ 10^6 cells. All the experiments were performed in triplicates and with untreated controls.

Pt content estimation in mitochondria: Nearly 10^6 A549 cells were seeded in 90 mm tissue culture plates. The cells were then treated with complexes **2** and **3** (5 µM) for 4 h in dark. The DMEM was removed, and cells were washed with DPBS. The cells were then detached using a cell scraper and the cell lysates were transferred to 50 ml Falcon tubes. The plates were thoroughly scraped to get maximum yield of mitochondria. The cells were centrifuged at 600 r.p.m at 4 °C for 10 min. The supernatant was discarded, and cells were re-suspended in mitochondrial isolation buffer IB (10 ml of 0.1M tris(hydroxymethyl)aminomethane (Tris)/3-(N-morpholine)propanesulfonic acid and 1 ml of ethylene glycol-bis(b-aminoethyl ether)-N,N,N',N'-tetraacetic acid/Tris to 20 ml of 1 M sucrose and volume made up to 100 ml (pH 7.4) and 1 ml EGTA/Tris to 20 ml of 1 M sucrose and volume made up to 100 ml (pH = 7.4). Cells were then homogenized at 4°C using a Teflon pestle (1600 r.p.m.) and the cell suspensions were stroked gently in a glass potter (initially cooled in ice-bath to maintain the mitochondrial integrity). The homogenate was then centrifuged at 600 r.p.m. at 4 °C for 10 min. The supernatant was collected and centrifuged at 7000 r.p.m. at 4 °C for 10 min. The supernatant was discarded, and the pellets were washed with 200 µl of ice-cold isolation buffer IB. The homogenate was centrifuged again at 7000 r.p.m. at 4 °C for 10 min and the

pellet containing mitochondria was collected. One such set was used for measuring the concentration by Biuret methods and examining the separation of mitochondria by gel electrophoresis. Another identical set was used for Pt estimation by diluting in 2% HNO_3-DPBS solutions by ICP-MS method.

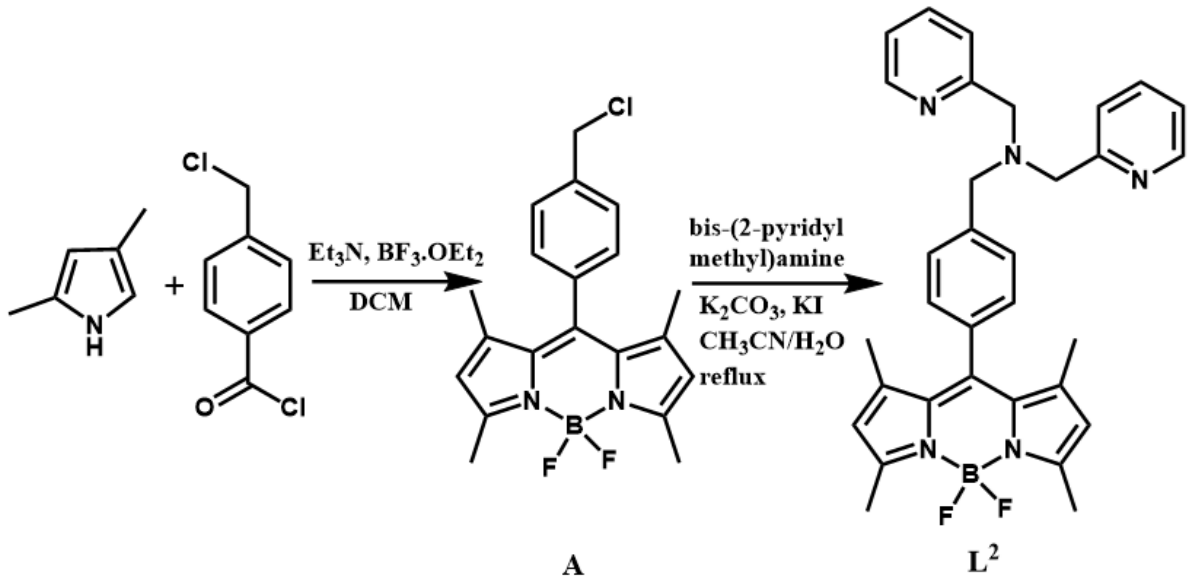

Scheme S1. Synthetic scheme for the preparation of ligand $\mathbf{L^2}$ (the molecular structure of precursor A is shown).

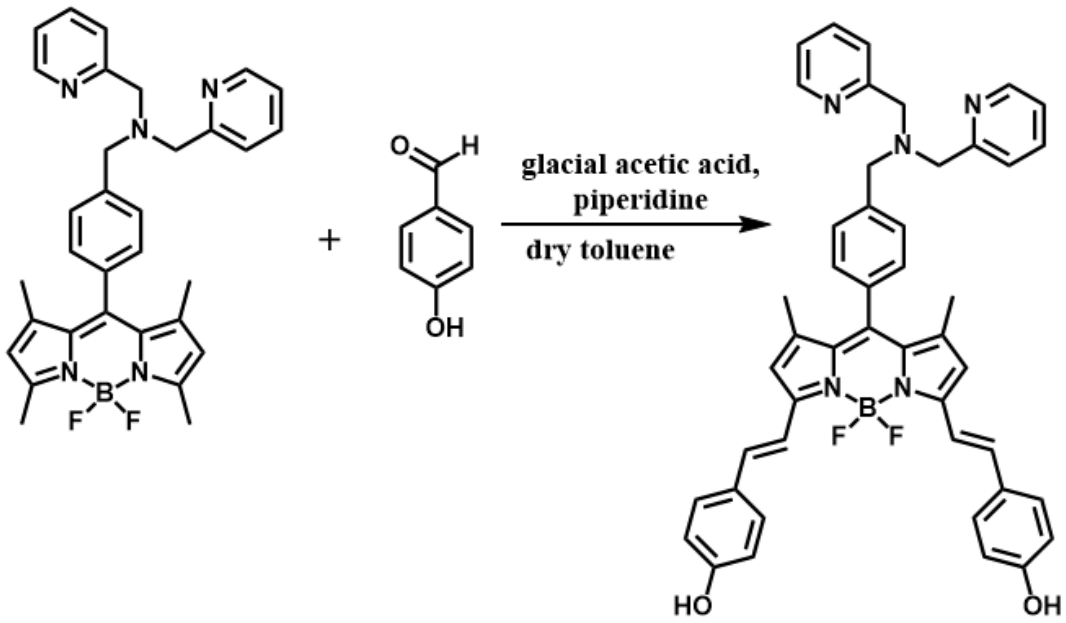

L^3

Scheme S2. Synthetic scheme for the preparation of ligand L^3.

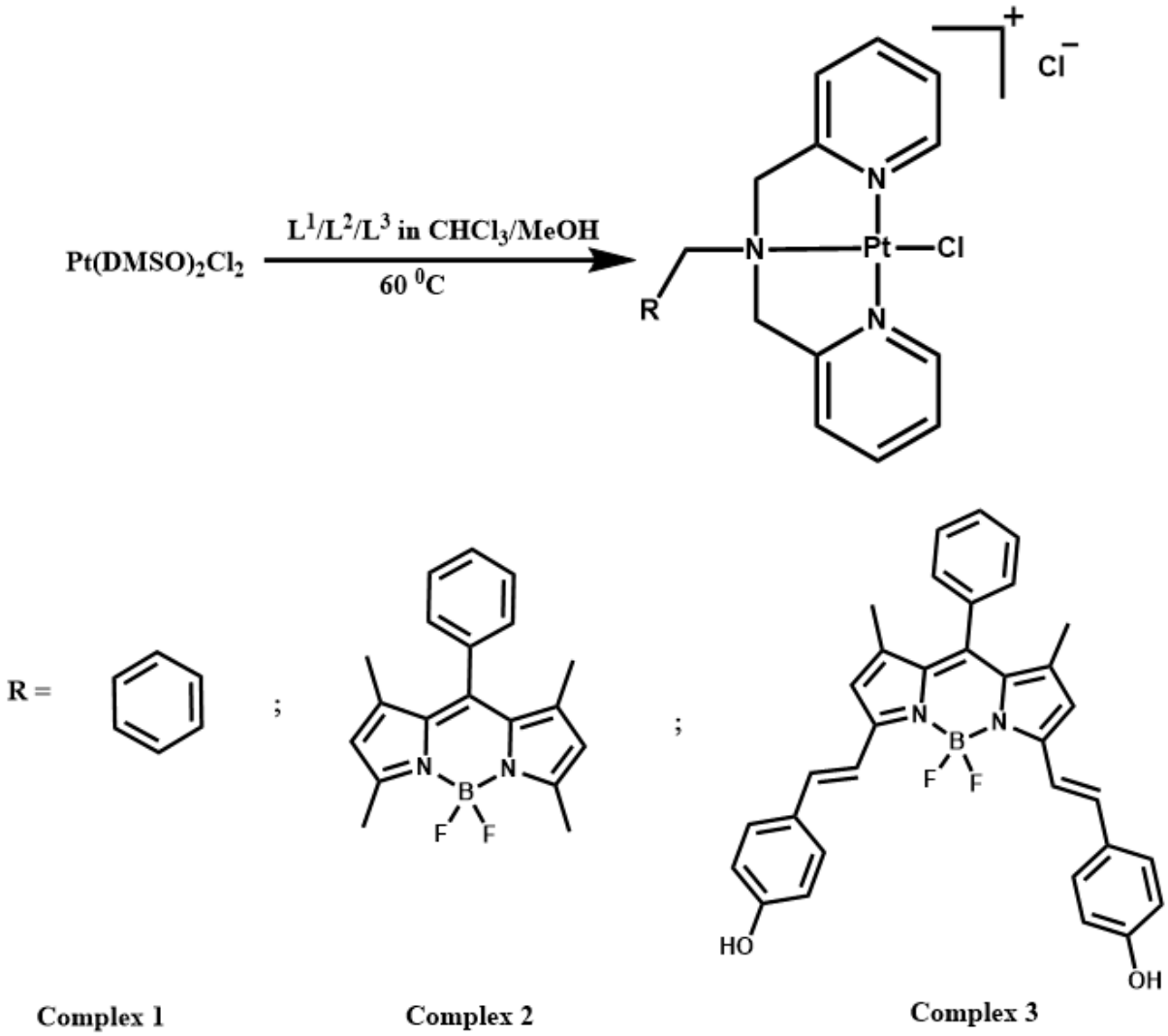

Scheme S3. Synthetic scheme for the preparation of complexes **1-3**.

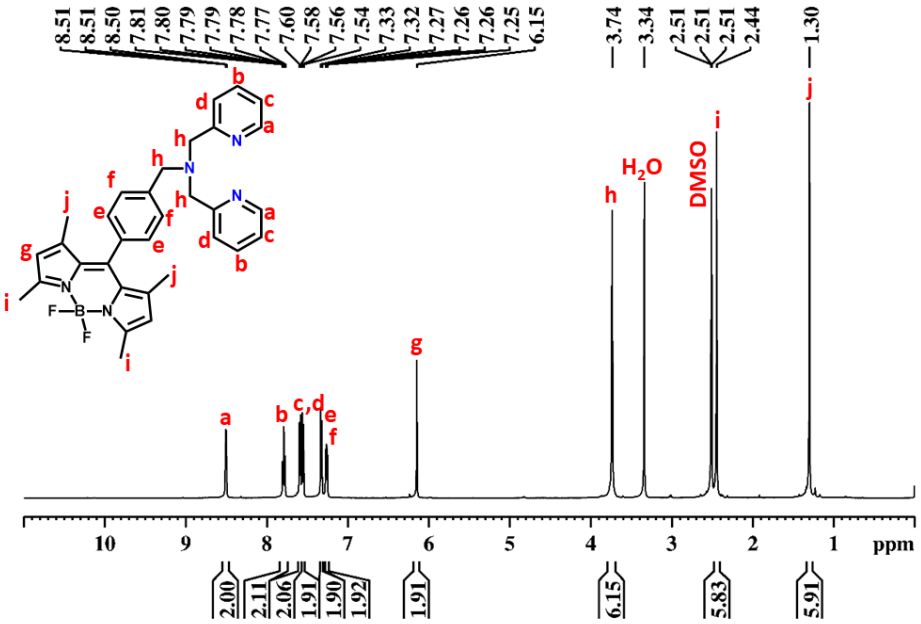

Figure S1. ^{1}H NMR spectrum of ligand **L^{2}** in DMSO-d$_6$.

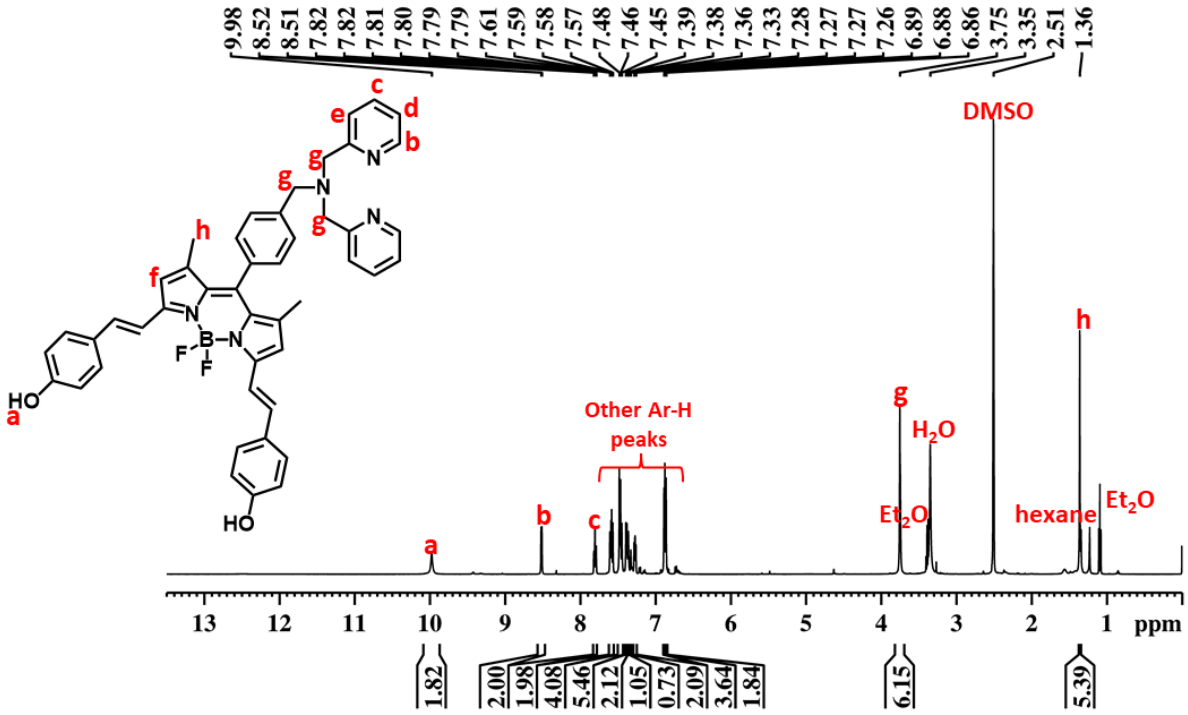

Figure S2. ^{1}H NMR spectrum of ligand **L^{3}** in DMSO-d$_6$.

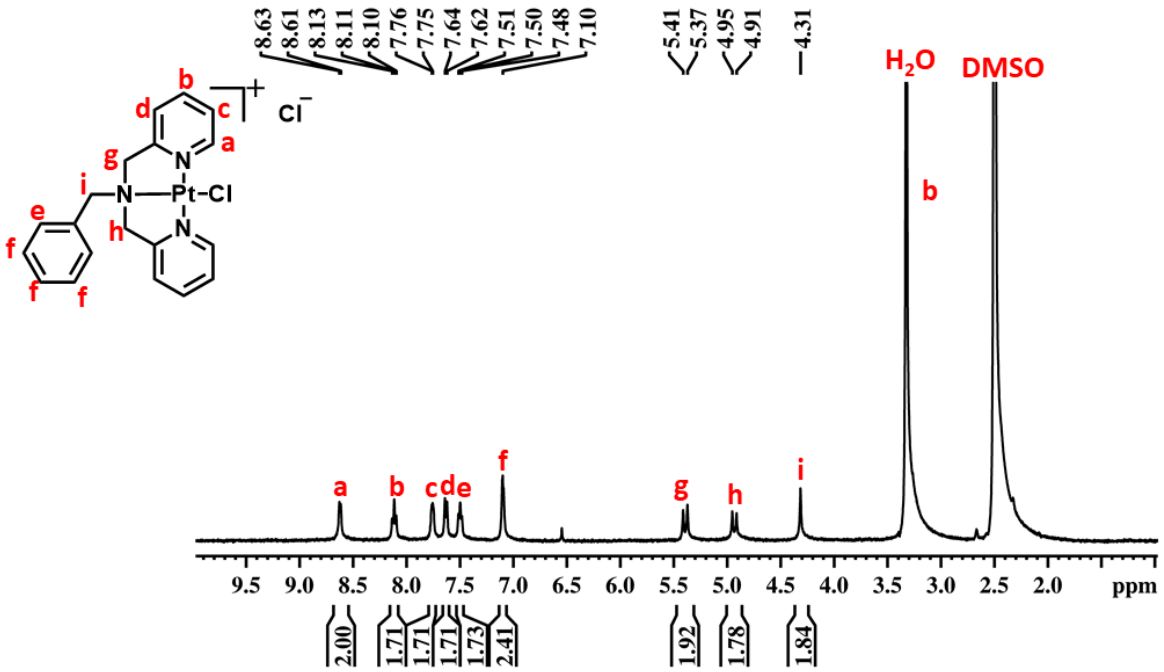

Figure S3. ^{1}H NMR spectrum of complex **1** in DMSO-d_6.

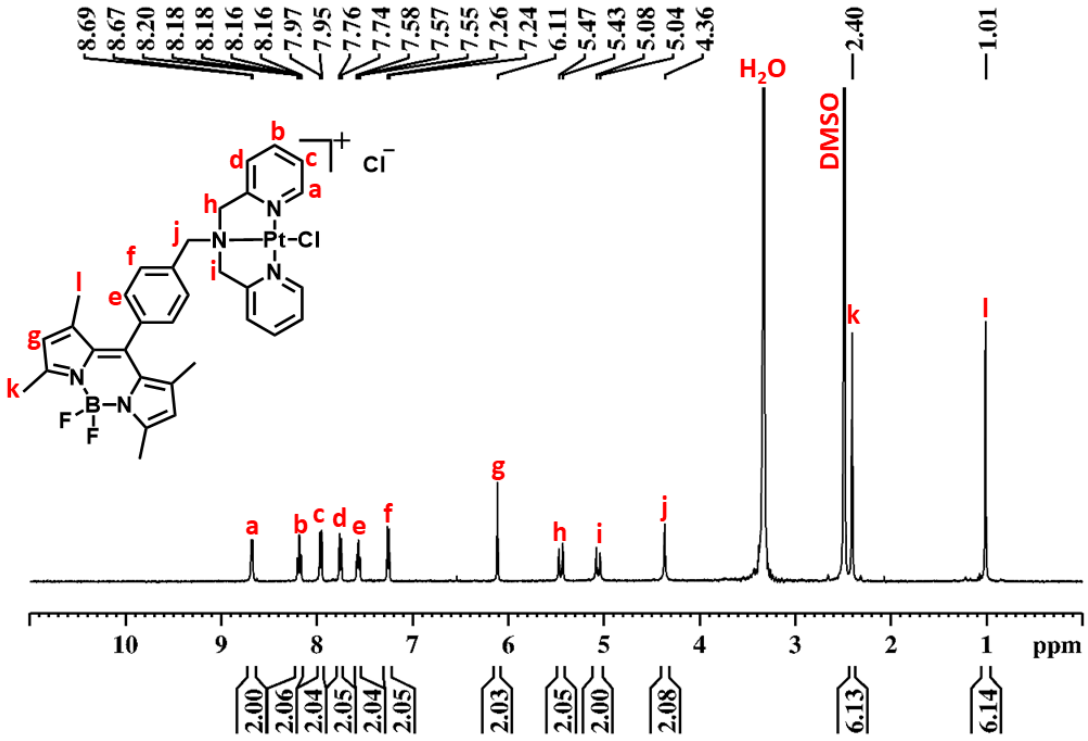

Figure S4. ^{1}H NMR spectrum of complex **2** in DMSO-d_6.

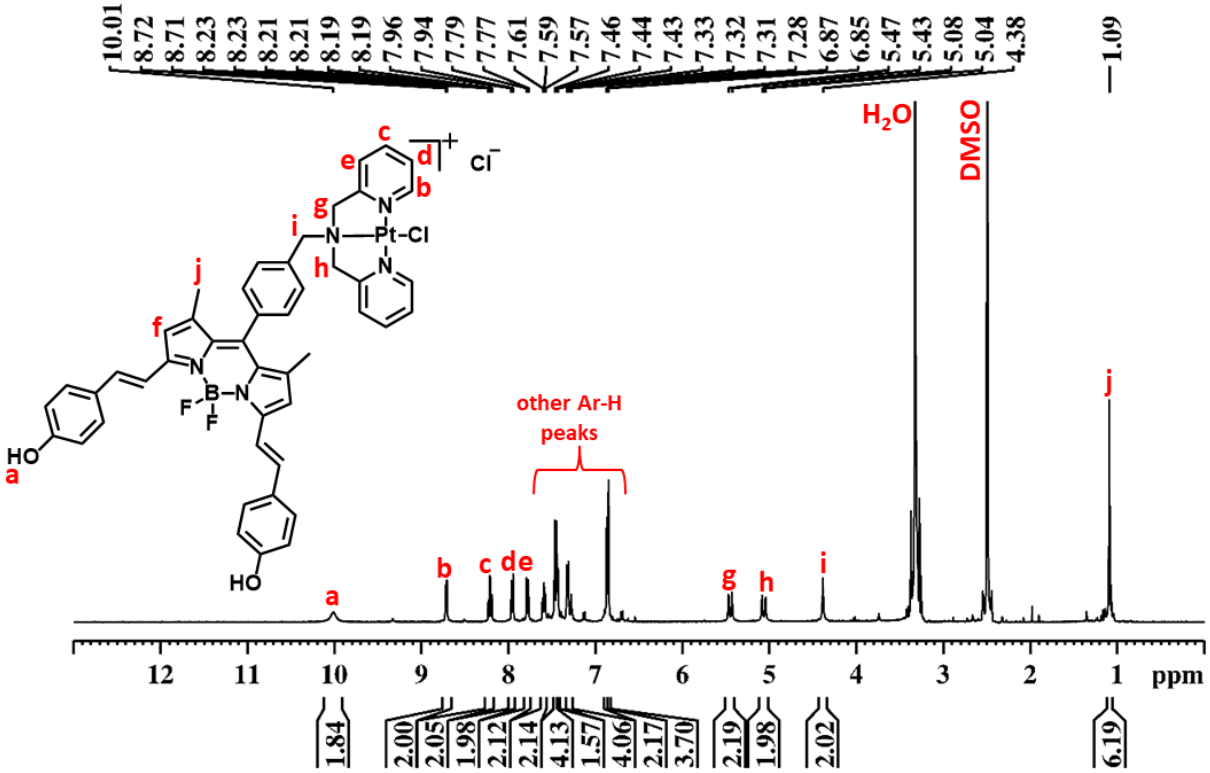

Figure S5. ^{1}H NMR spectrum of complex **3** in DMSO-d_6.

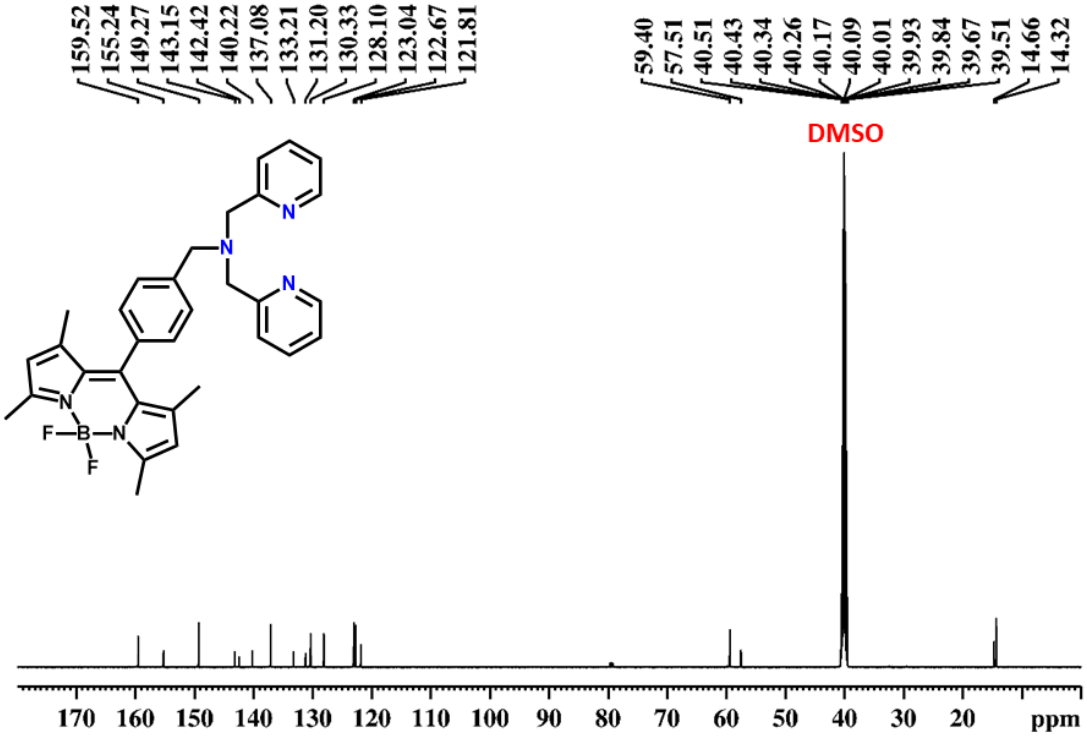

Figure S6. ^{13}C NMR spectrum of ligand **L²** in DMSO-d_6.

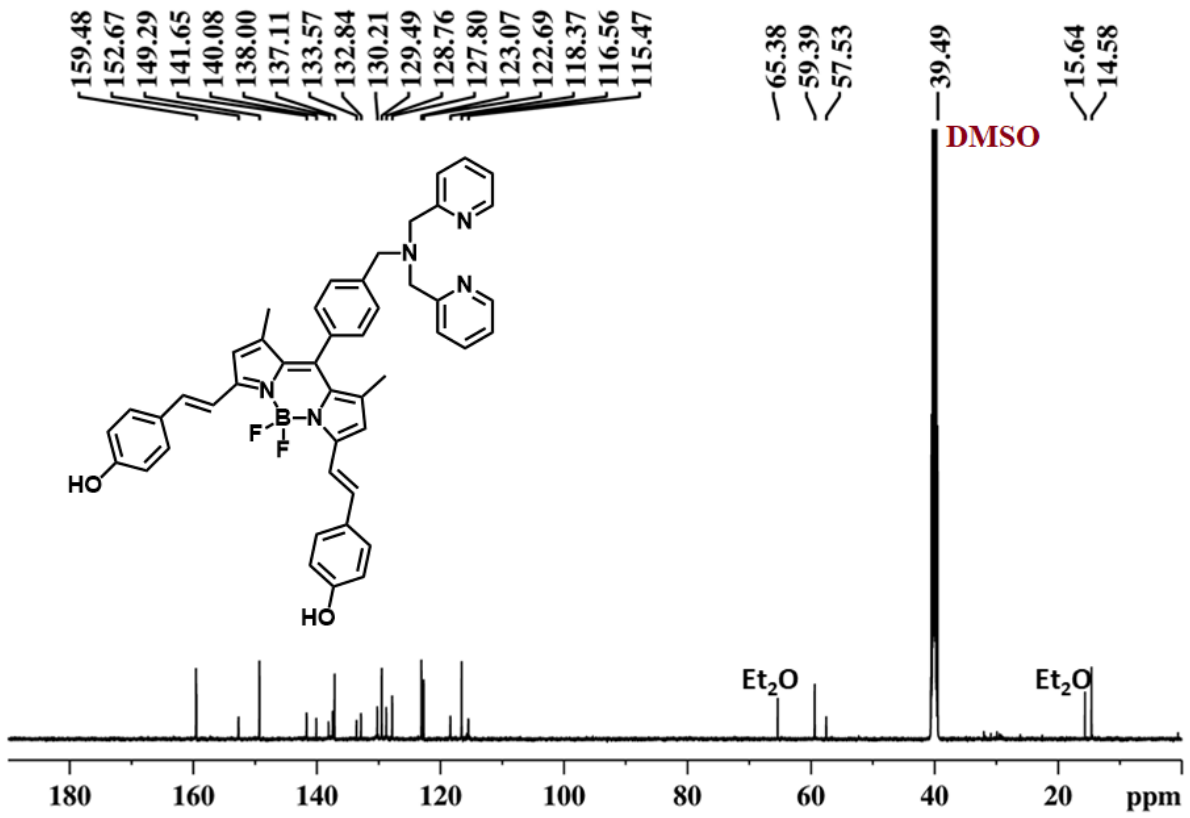

Figure S7. ^{13}C NMR spectrum of ligand $\mathbf{L^3}$ in DMSO-d_6.

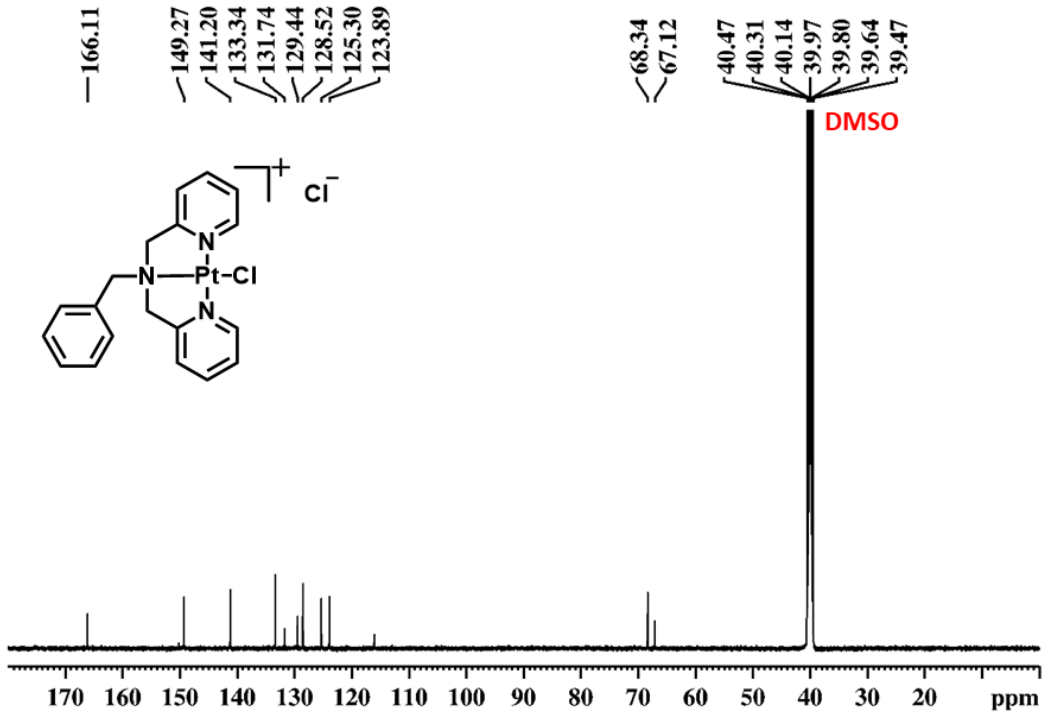

Figure S8. ^{13}C NMR spectrum of complex **1** in DMSO-d_6.

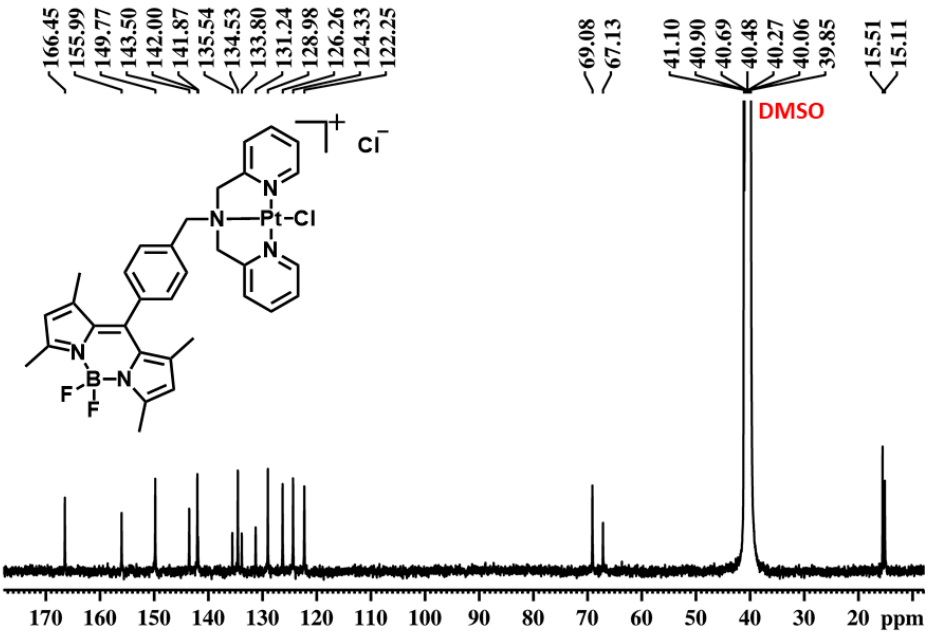

Figure S9. ^{13}C NMR spectrum of complex **2** in DMSO-d_6.

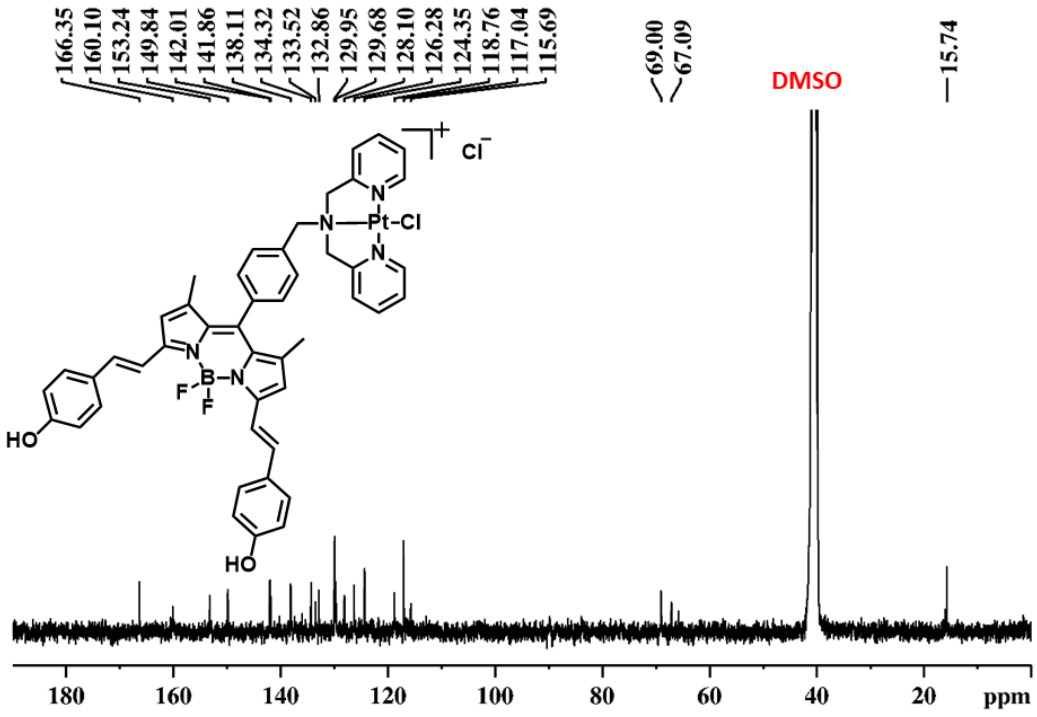

Figure S10. ^{13}C NMR spectrum of complex **3** in DMSO-d_6.

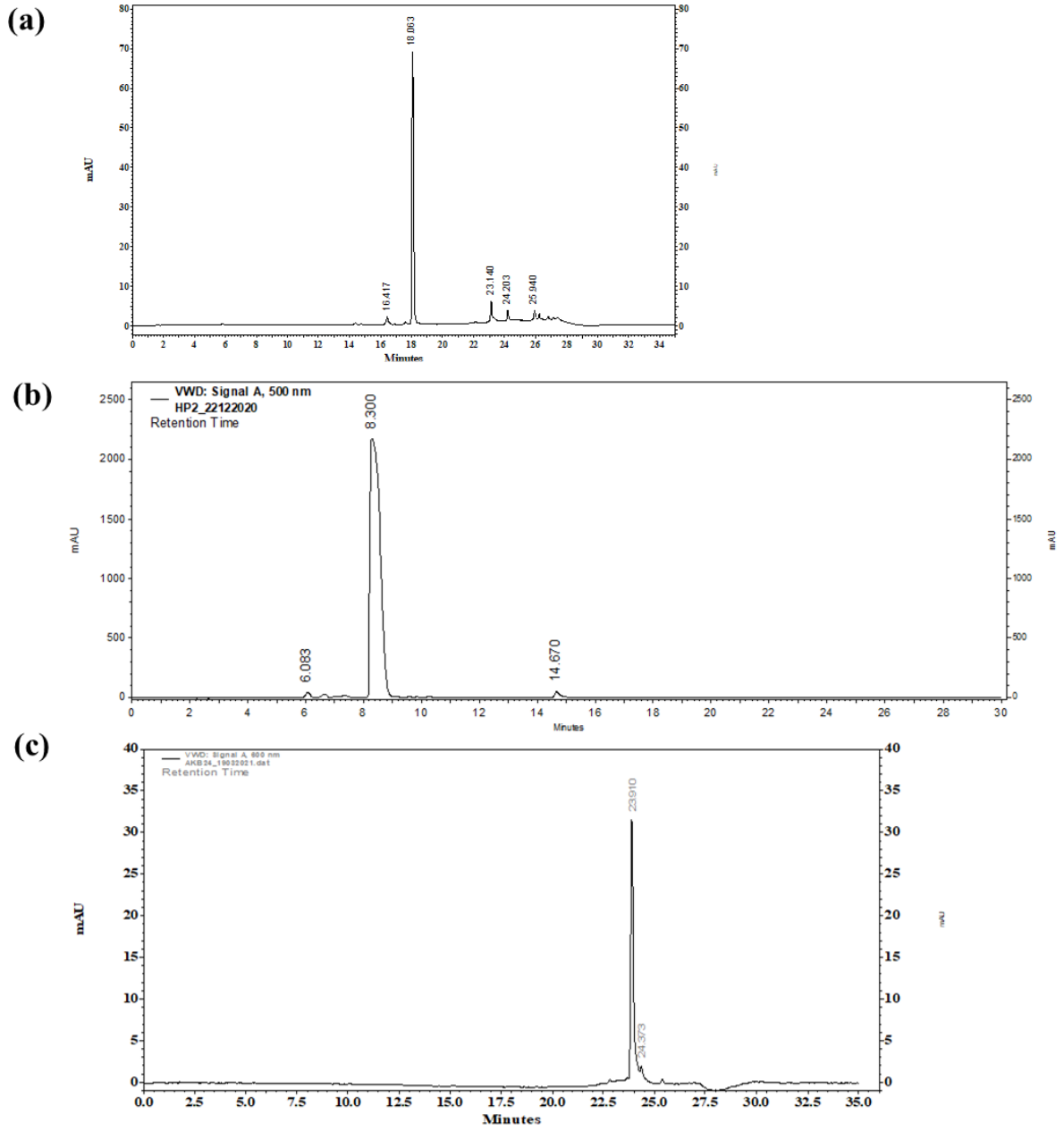

Figure S11. HPLC chromatograms for purity check (a) for complex **1,** (b) for complex **2** and (c) for complex **3**. Method details: HPLC: Hypersil GOLD (150×4.6), 3 micron, Mobile phase: methanol/water; Flow rate: 0.8 mL/min; injection volume: 15 µL. Detector wavelength: 254 nm (for complex 1); 500 nm (for complex 2); 600 nm(for complex 3).

Change in volume of methanol and water with time is shown below:

Time (min)	Flow rate (mL/min)	Mobile phase water volume	Mobile phase methanol
0	0.8	40	60
2	0.8	40	60
15	0.8	0	100
20	0.8	0	100
22	0.8	40	60

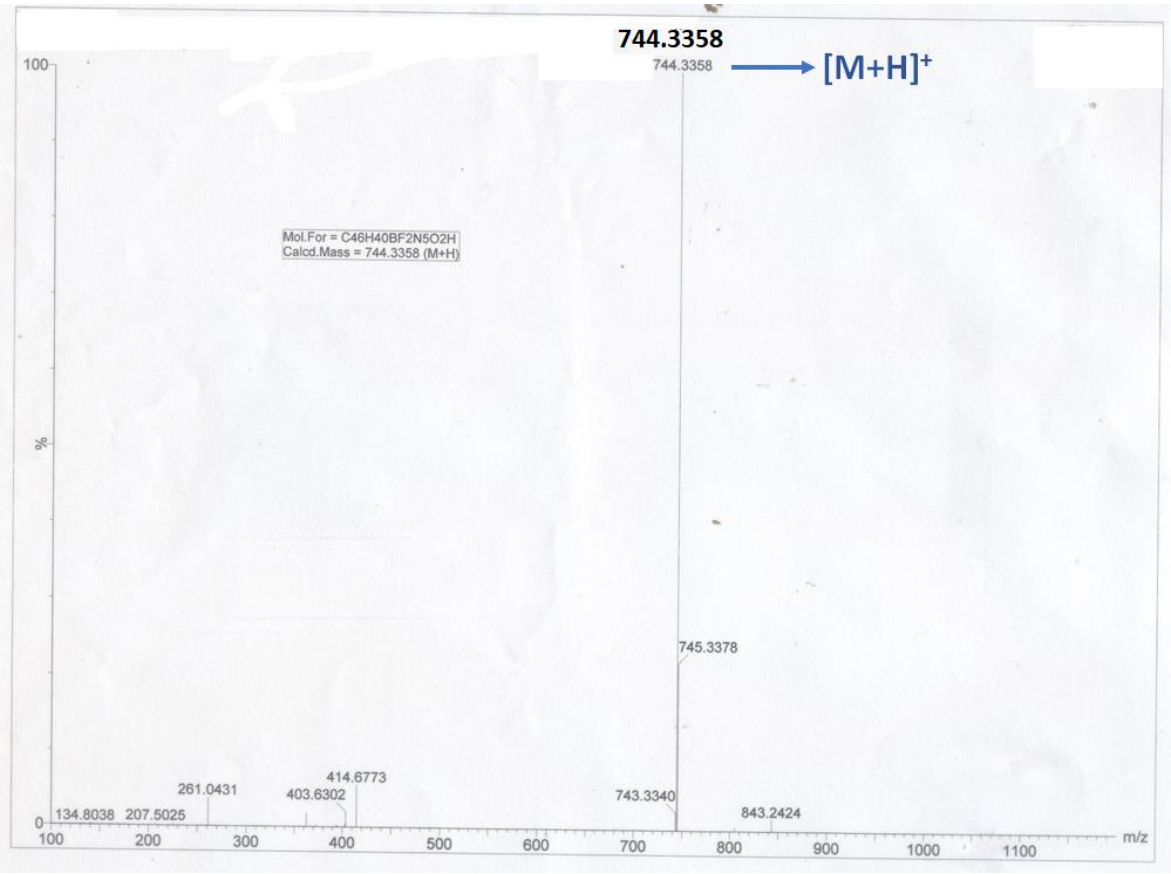

Figure S12. Mass spectrum of ligand $\mathbf{L^3}$ recorded in acetonitrile with peak corresponding to $[M+H]^+$ (m/z) at 744.3358.

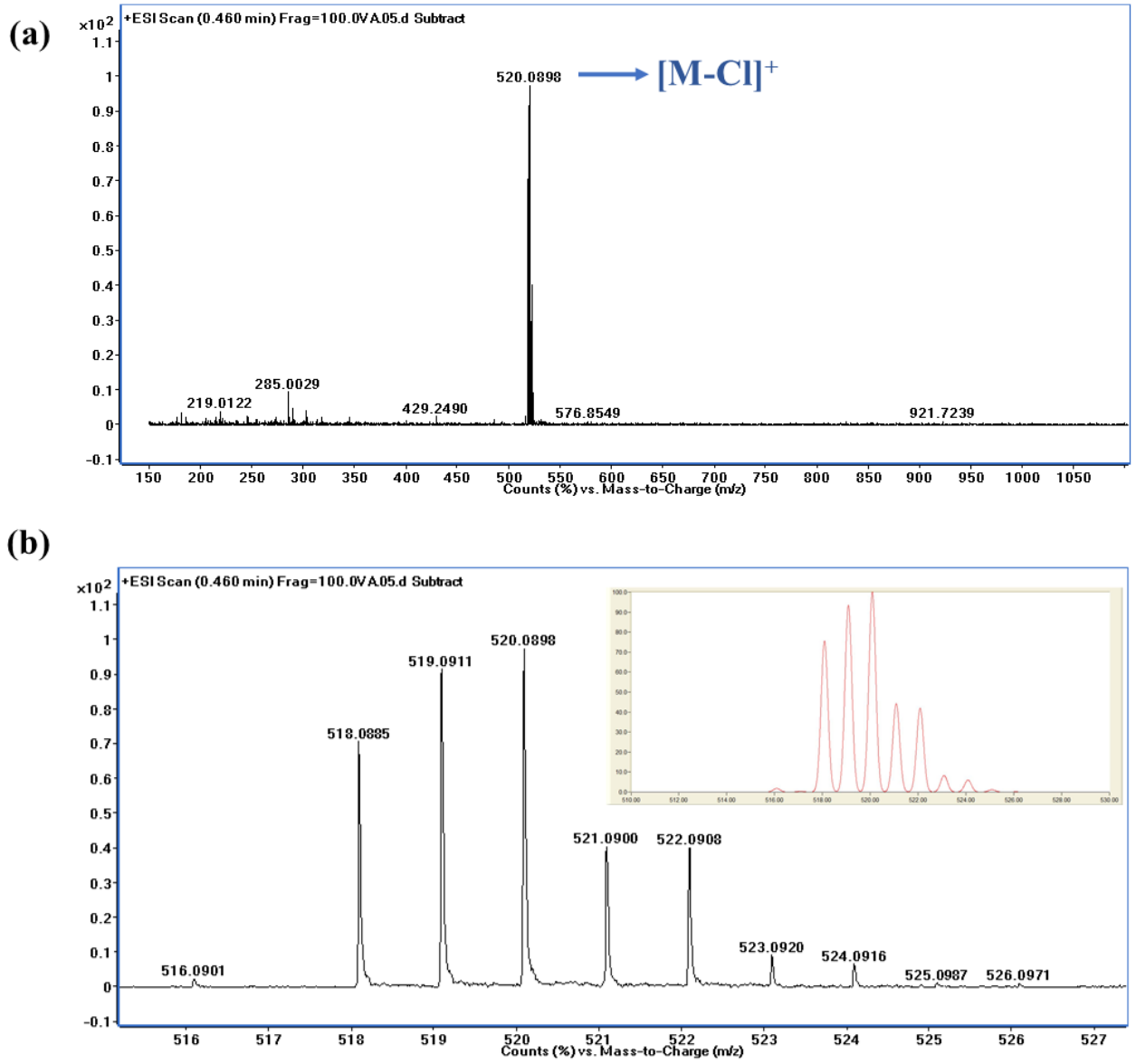

Figure S13. (a) Mass spectrum of complex **1** recorded in methanol with peak corresponding to $[M-Cl]^+$ (m/z) at 520.0898. (b) Isotopic distribution of the complex indicating unipositive charge of the complex. Inset shows simulated isotopic distribution pattern.

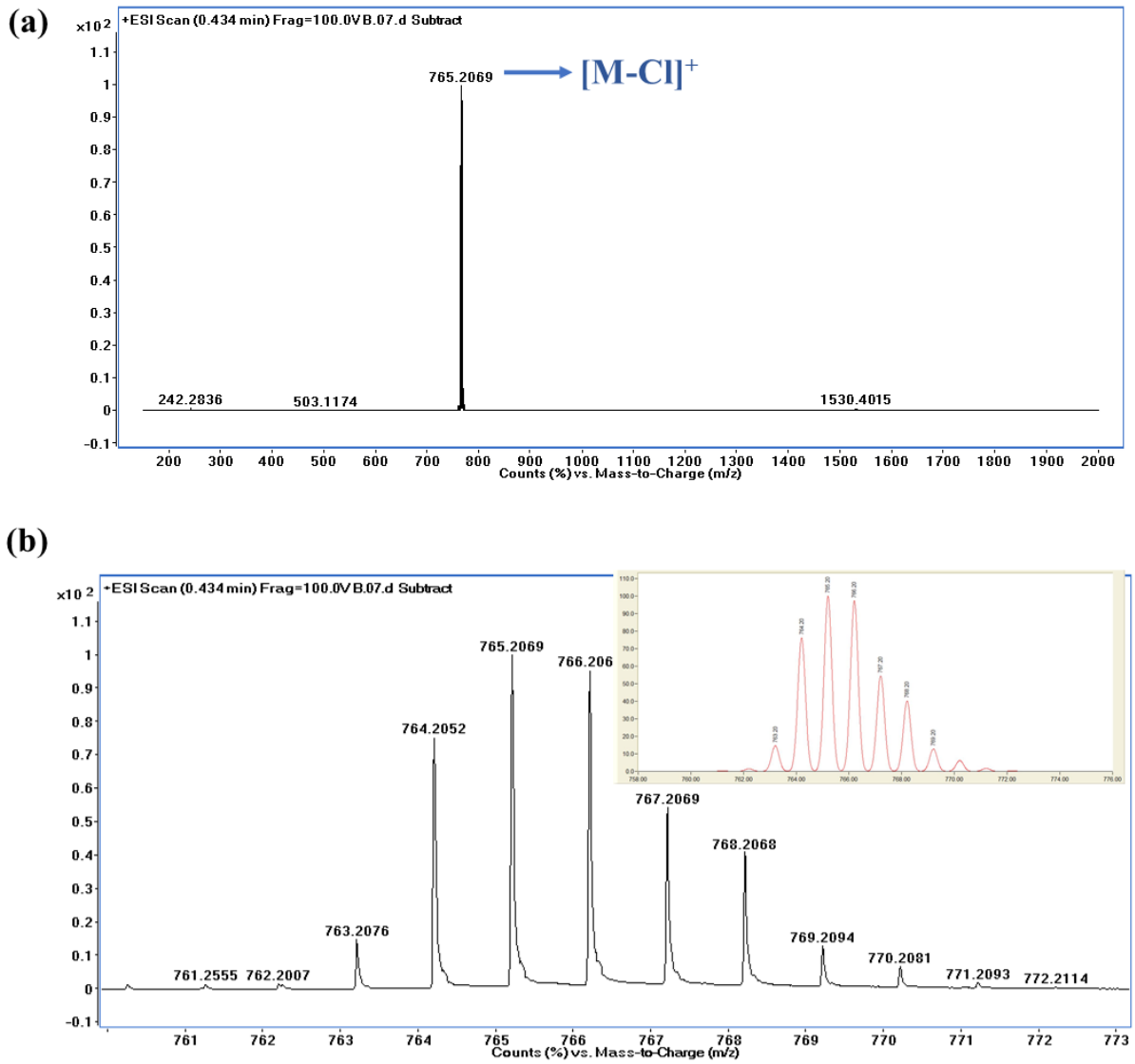

Figure S14. (a) Mass spectrum of complex **2** recorded in methanol with peak corresponding to $[M\text{-}Cl]^+$ (m/z) at 765.2069. (b) Isotopic distribution of the complex indicating unipositive charge of the complex. Inset shows simulated isotopic distribution pattern.

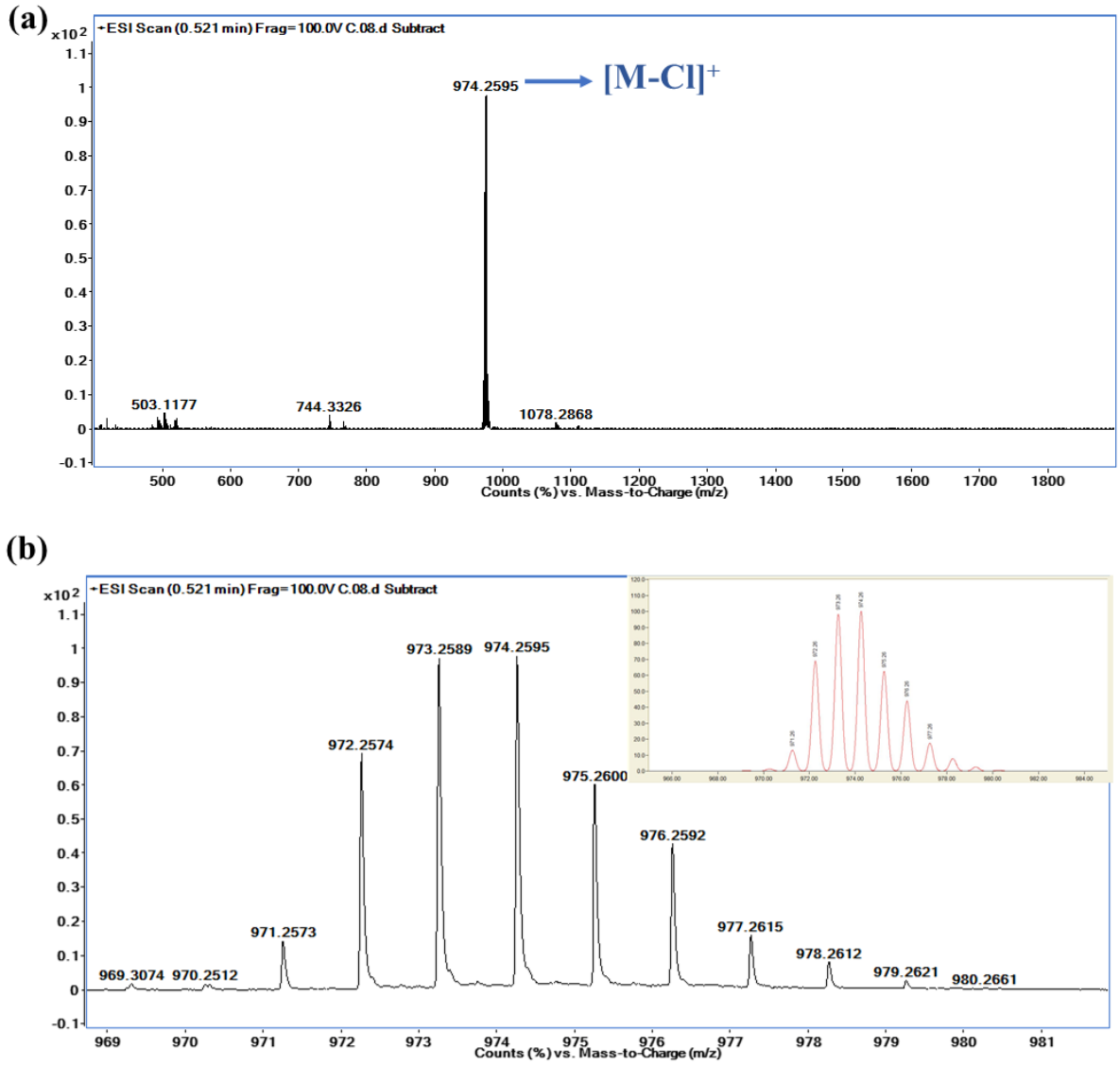

Figure S15. (a) Mass spectrum of complex **3** recorded in methanol with peak corresponding to $[M\text{-}Cl]^+$ (m/z) at 974.2595. (b) Isotopic distribution of the complex indicating unipositive charge of the complex. Inset shows simulated isotopic distribution pattern.

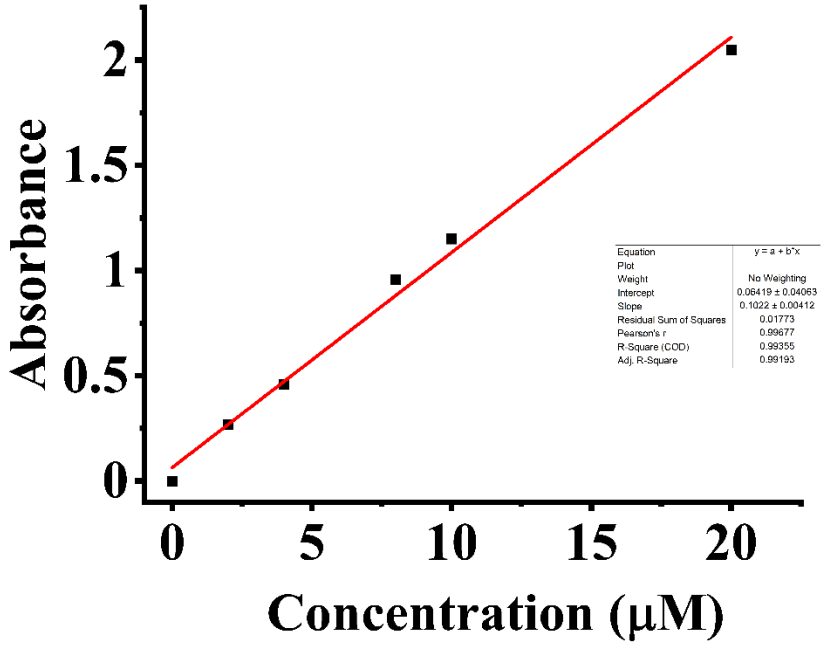

Figure S16. UV-vis spectra of complex **3** recorded at different concentrations and absorbance was plotted against concentration.

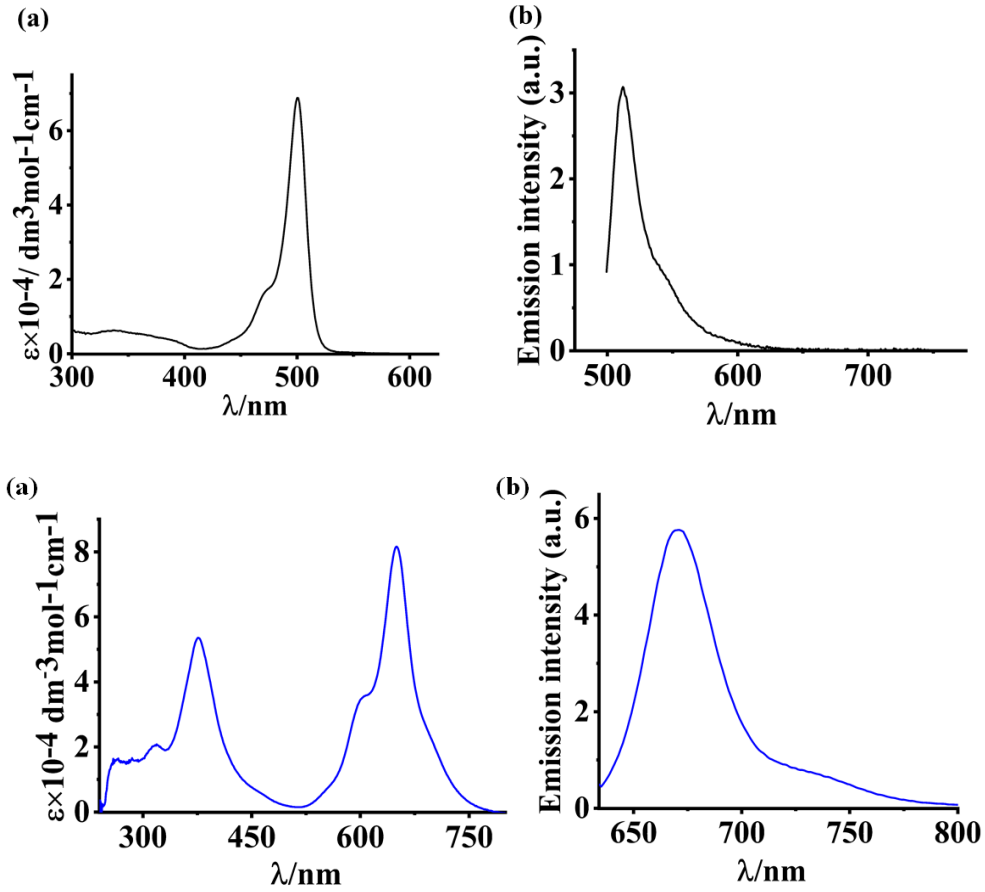

Figure S17. (a) Absorption and (b) emission spectra of ligand $\mathbf{L^2}$ in 1:1 (v/v) DMSO/DPBS. (c) Absorption and (d) emission spectra of ligand $\mathbf{L^3}$ in 1:1 (v/v) DMSO/DPBS.

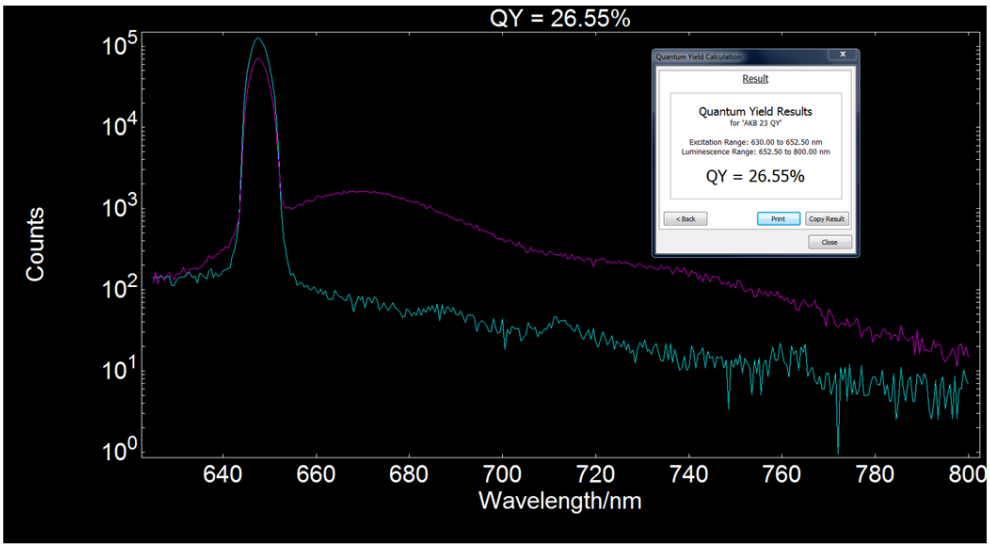

Figure S18. Fluorescence quantum yield for $\mathbf{L^3}$ in DMF.

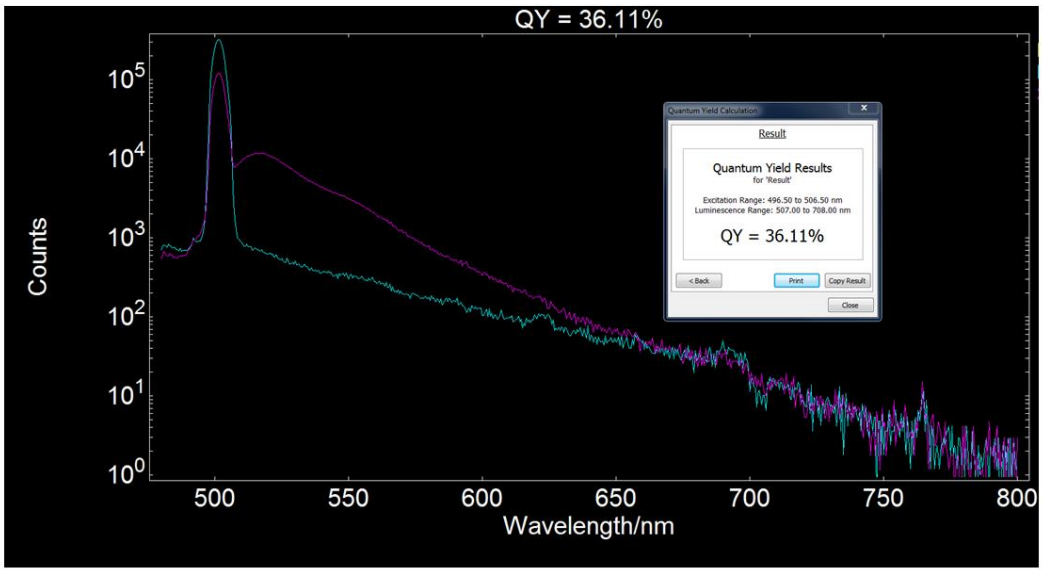

Figure S19. Fluorescence quantum yield for complex **2** in DMF.

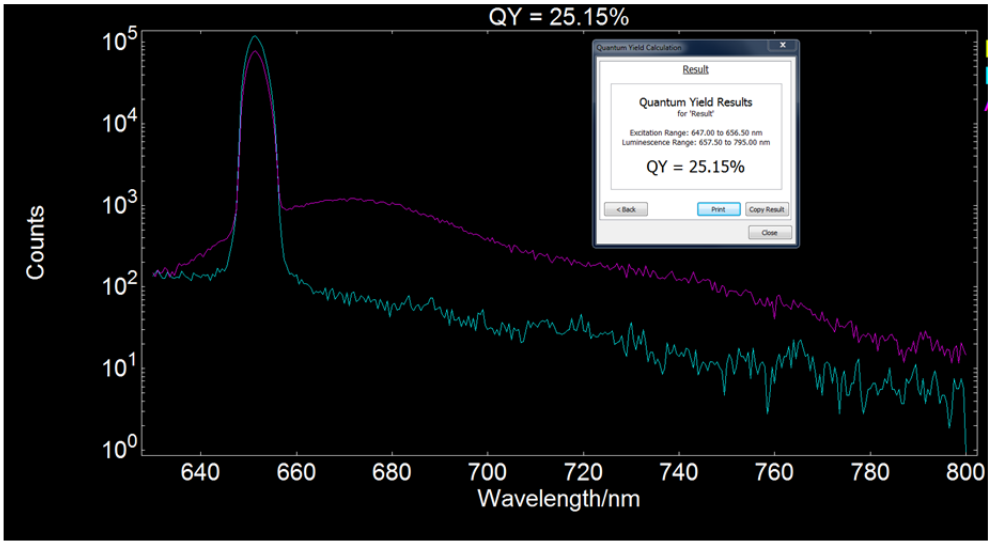

Figure S20. Fluorescence quantum yield for complex **3** in DMF.

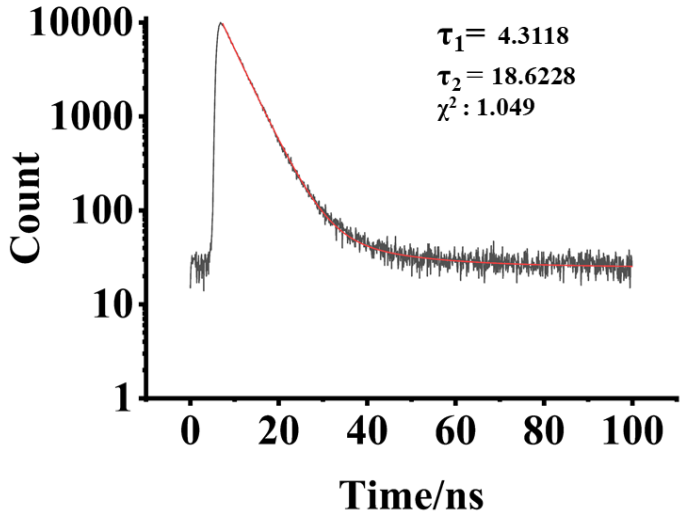

Figure S21. Lifetime decay profile for lifetime measurement of complex **2** in DMF.

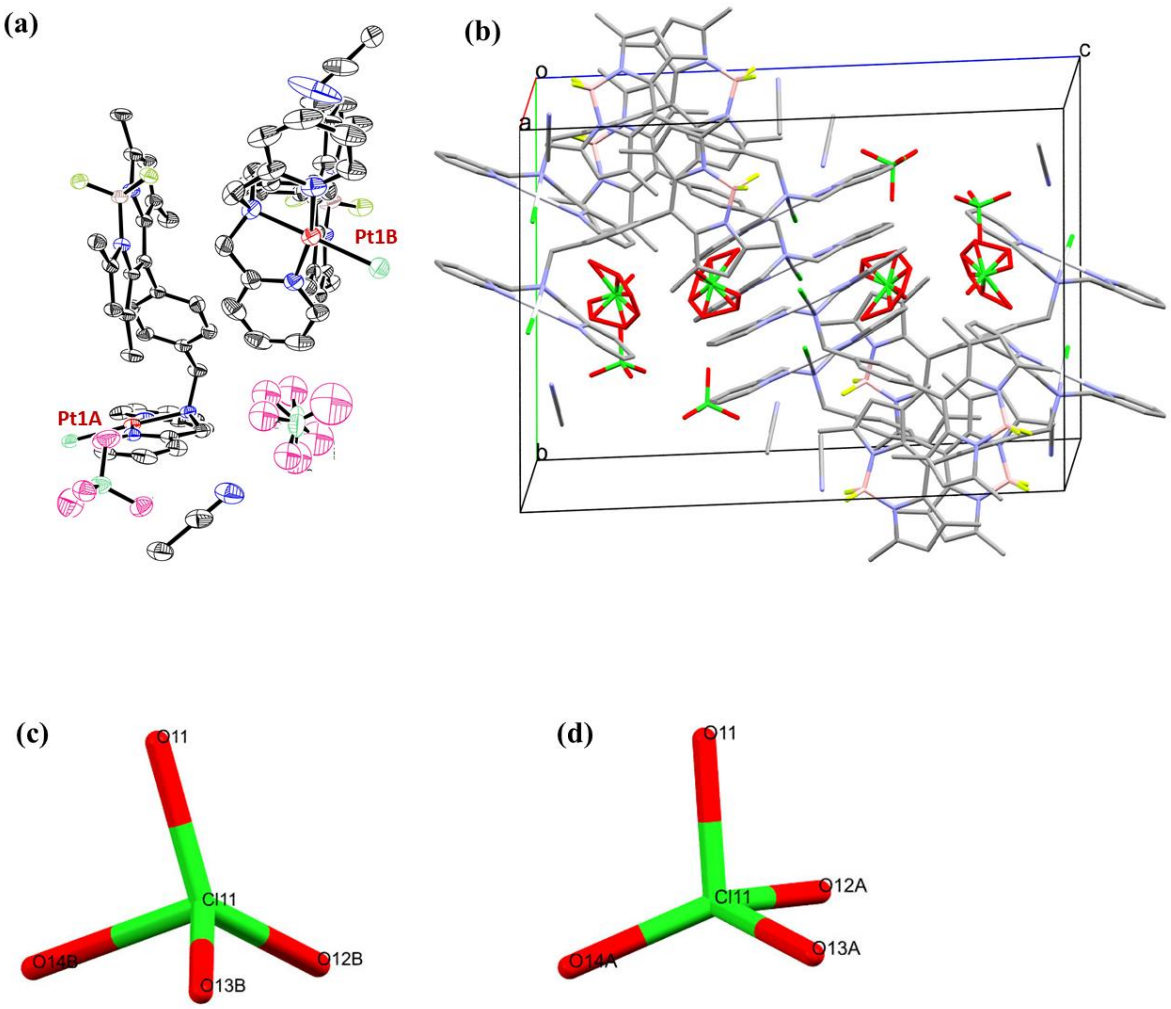

Figure S22. (a) ORTEP diagram of two molecules of complex **2a** in the crystallographic asymmetric unit. One perchlorate anion oxygen atom positional disorder is shown. Colour codes used: platinum, red; carbon, black; nitrogen, blue; boron, ivory; fluorine, light green; chlorine, deep green. (b) Unit cell packing diagram showing the presence of solvent of crystallization (c, d) view of disordered perchlorate along O11-C11, C_3 axis.

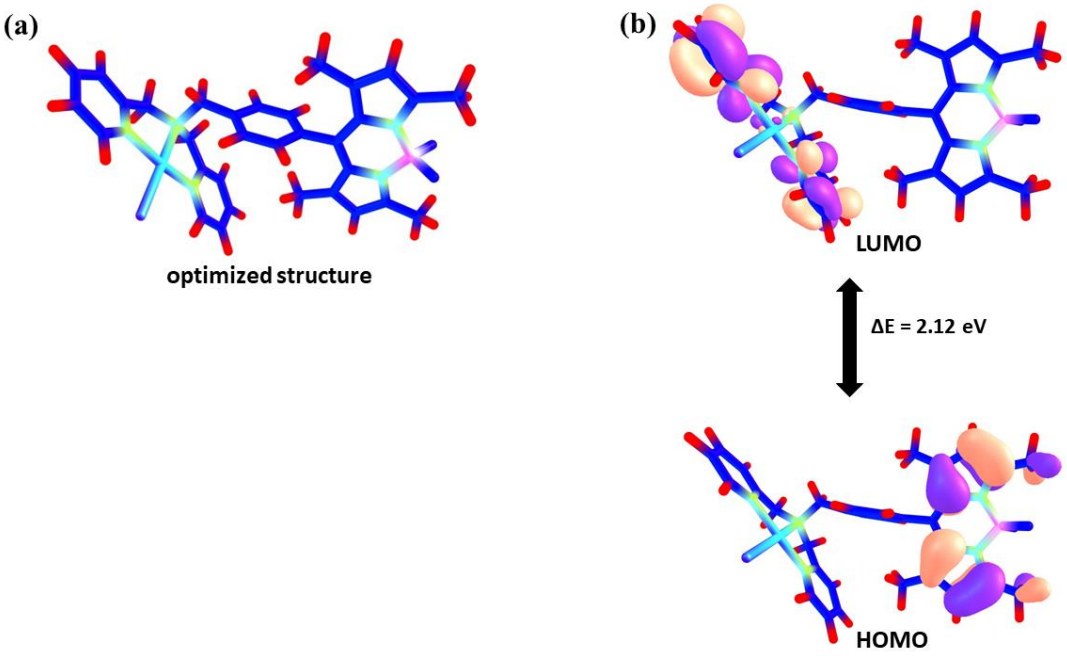

Figure S23. (a) Optimized structure and (b) nodal patterns of HOMO and LUMO of complex **2** as generated over optimized structure.

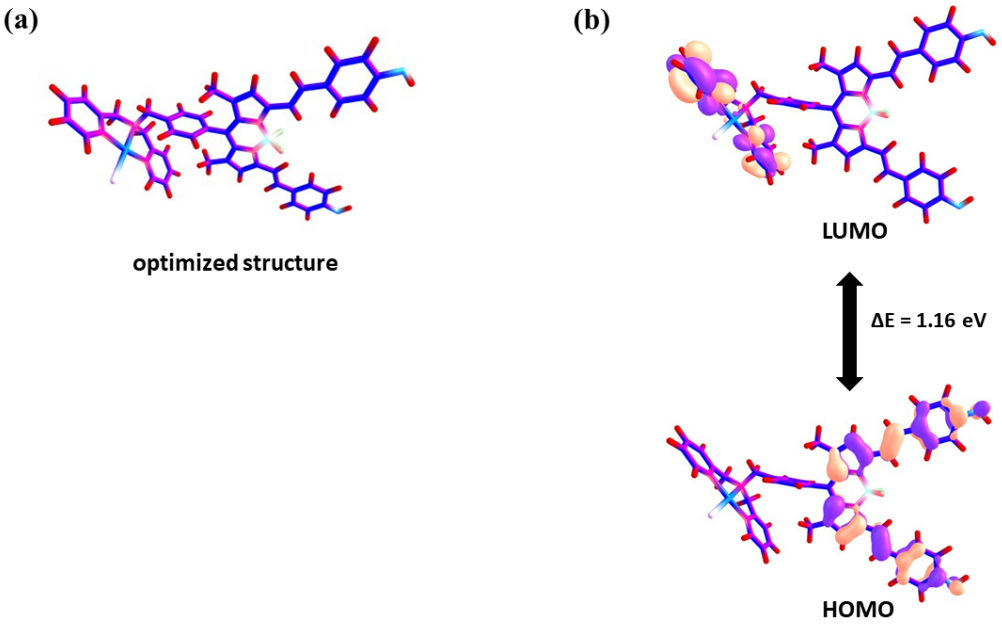

Figure S24. (a) Optimized structure and (b) nodal patterns HOMO and LUMO of complex **3** as generated over optimized structure.

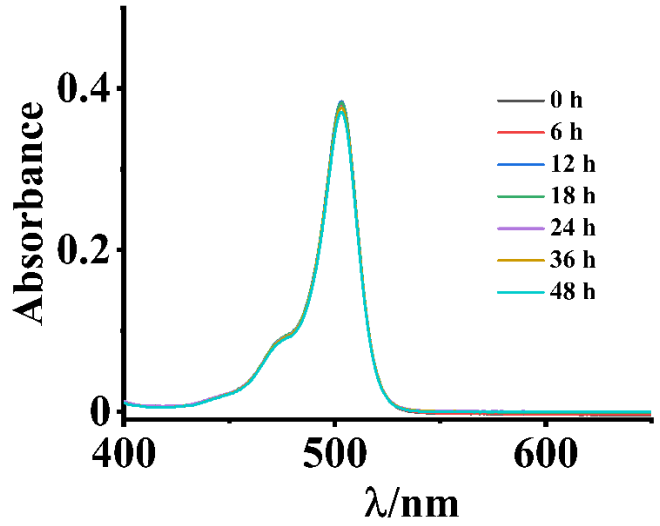

Figure S25. Time-dependent stability studies of complex **2** in 1:1 (v/v) DMSO/DPBS under dark condition.

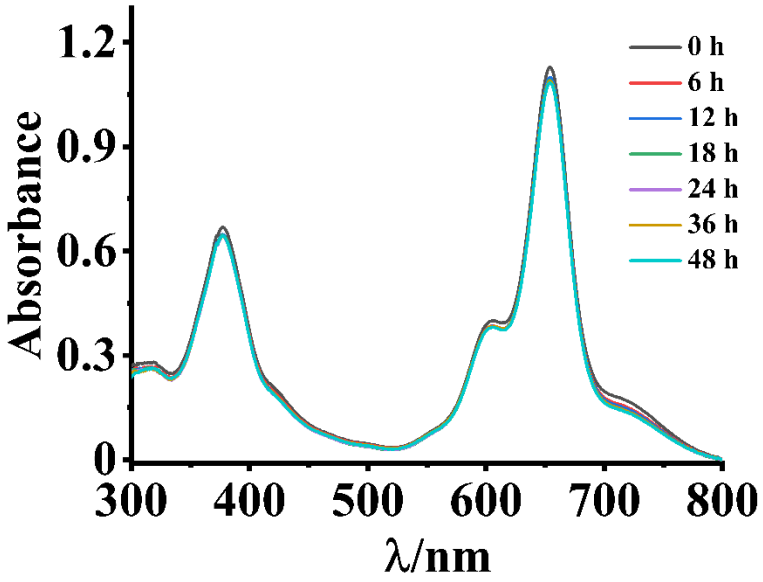

Figure S26. Time-dependent stability studies of complex **3** in 1:1 (v/v) DMSO/DPBS under dark condition.

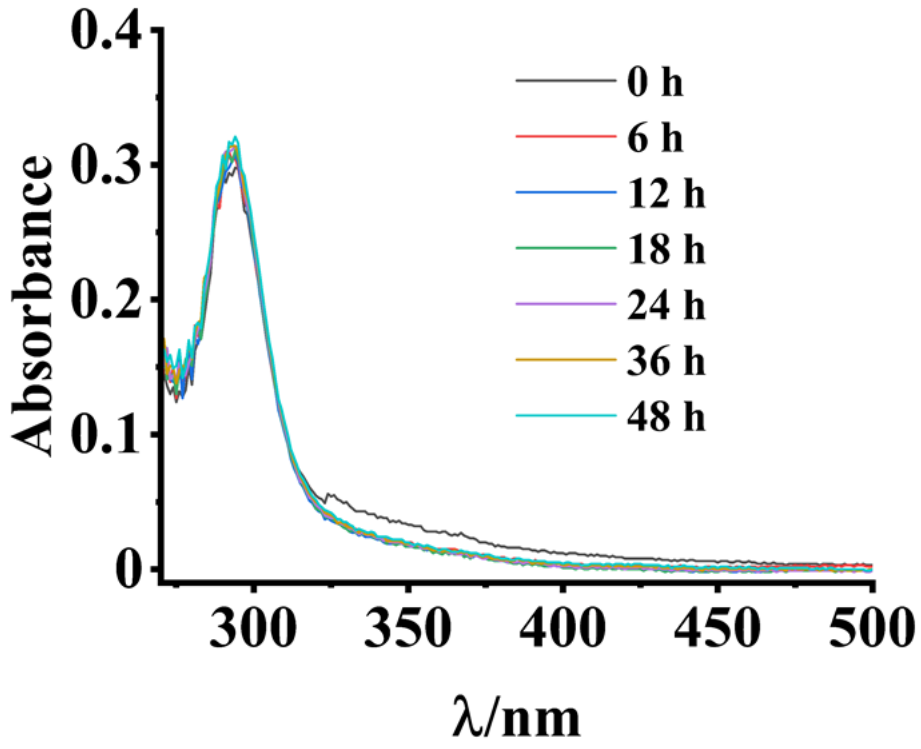

Figure S27. Time-dependent stability studies of complex **1** in 10% DMSO/DMEM under dark condition.

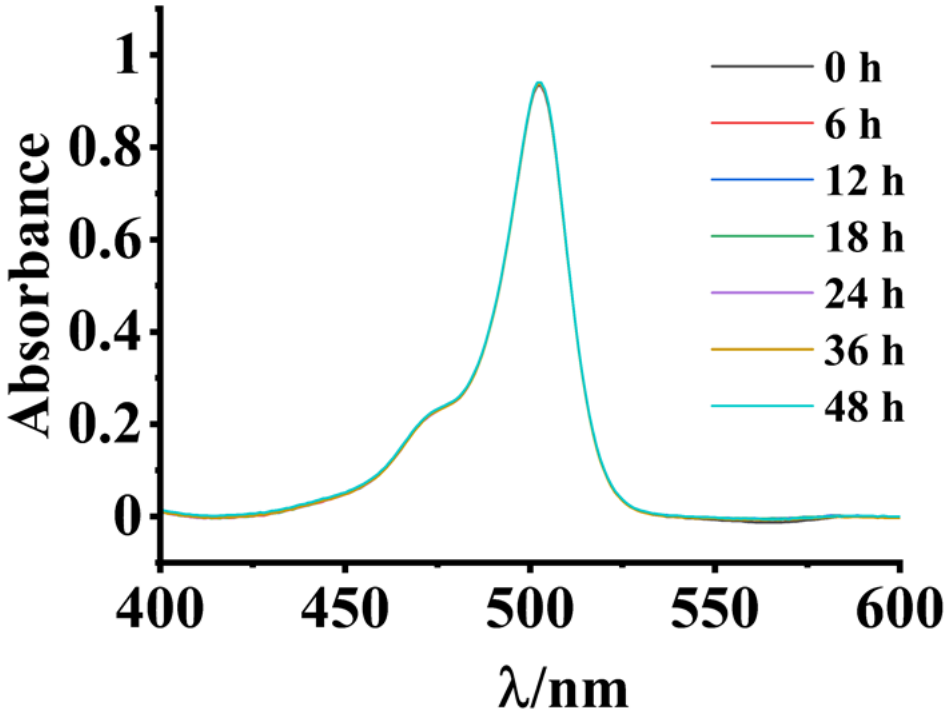

Figure S28. Time-dependent stability studies of complex **2** in 10% DMSO/DMEM under dark condition.

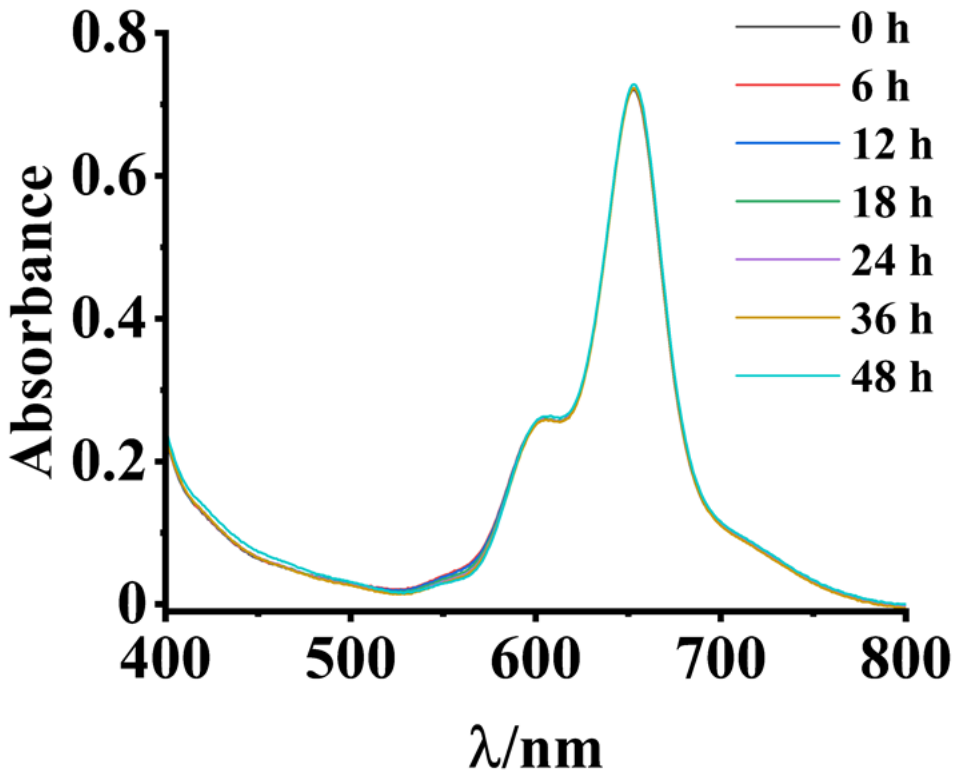

Figure S29. Time-dependent stability studies of complex **3** in 10% DMSO/DMEM under dark condition.

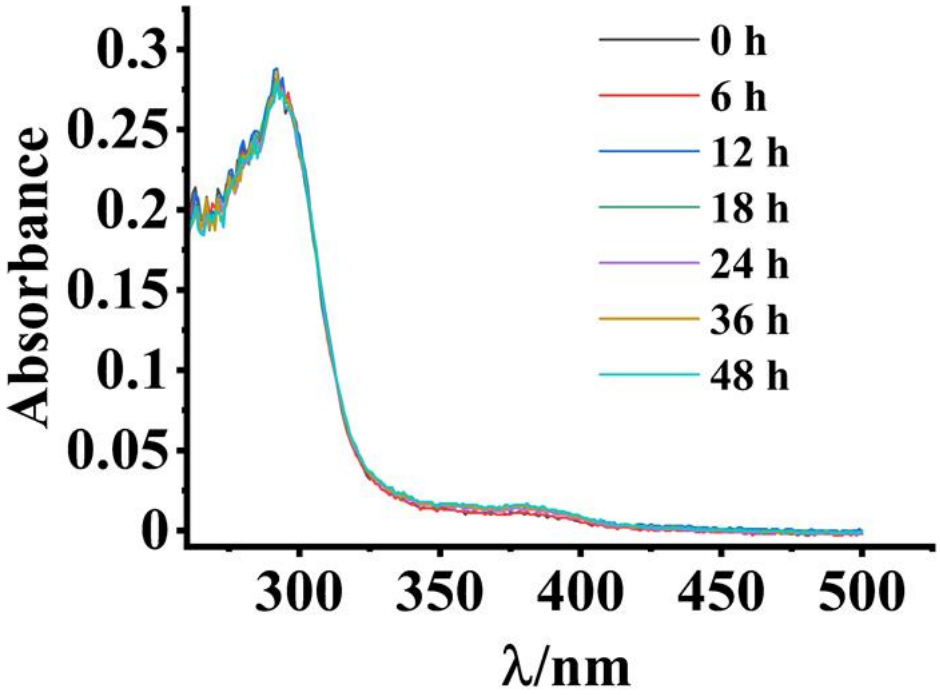

Figure S30. Time-dependent stability studies of complex **1** in presence of 10 equiv. GSH under dark condition.

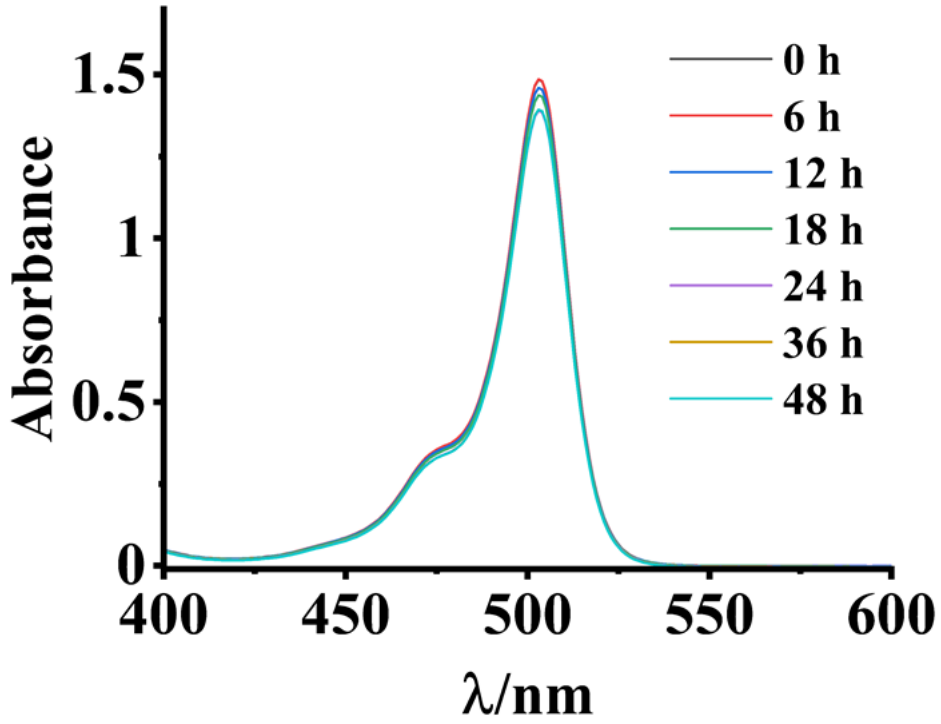

Figure S31. Time-dependent stability studies of complex **2** in presence of 10 equiv. GSH under dark condition.

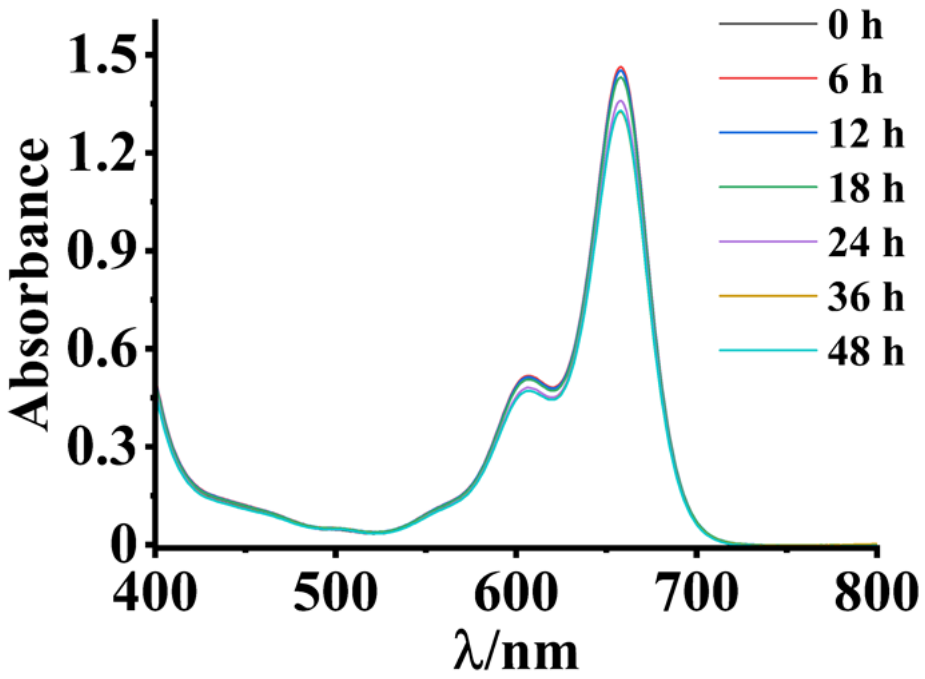

Figure S32. Time-dependent stability studies of complex **3** in presence of 10 equiv. GSH under dark condition.

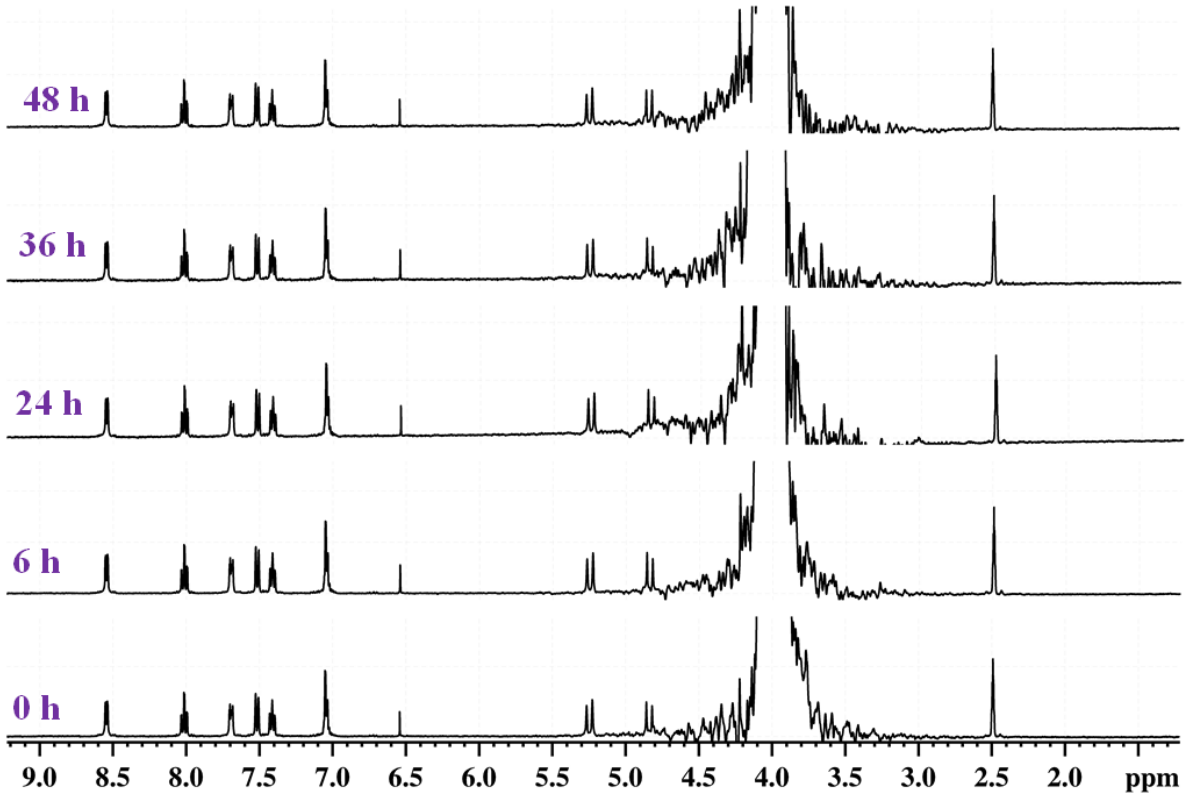

Figure S33. Time-dependent stability studies by ^{1}H NMR of complex **1** in DMSO-d_6-DPBS mixture under dark condition.

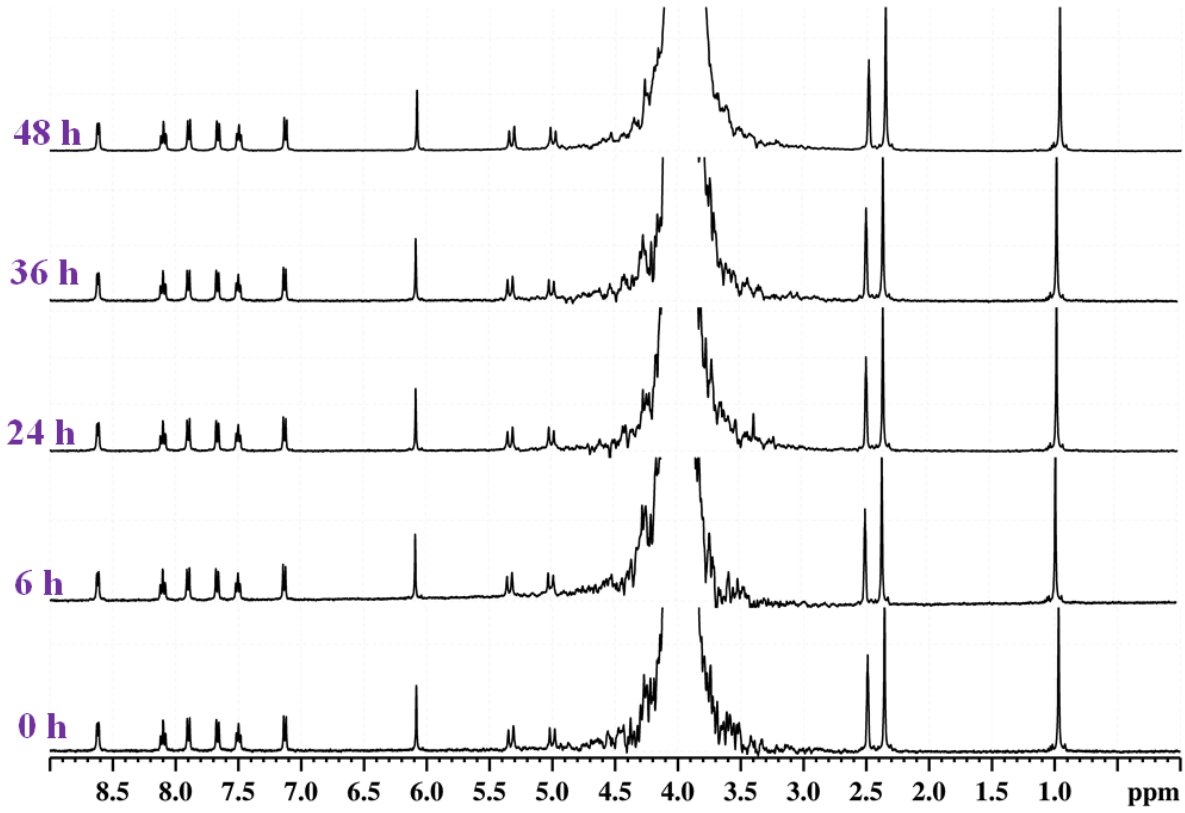

Figure S34. Time-dependent stability studies by ^{1}H NMR of complex **2** in DMSO-d_6-DPBS mixture under dark condition.

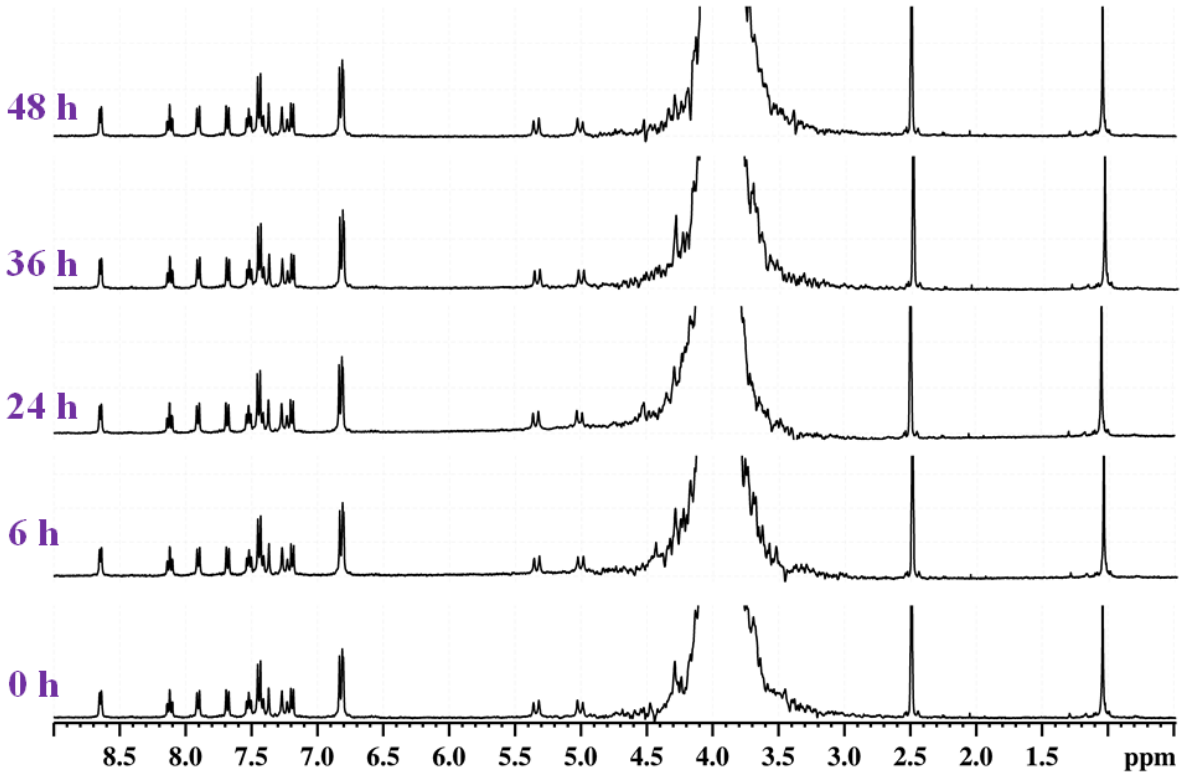

Figure S35. Time-dependent stability studies by ^{1}H NMR of complex **3** in DMSO-d_6-DPBS mixture under dark condition.

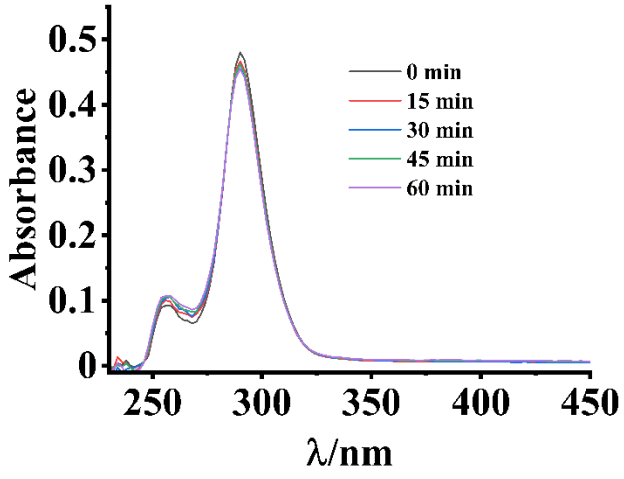

Figure S36. Photostability studies of complex **1** in 10% DMSO/DPBS (dose: 10 J/cm^2, 400-700 nm wavelength).

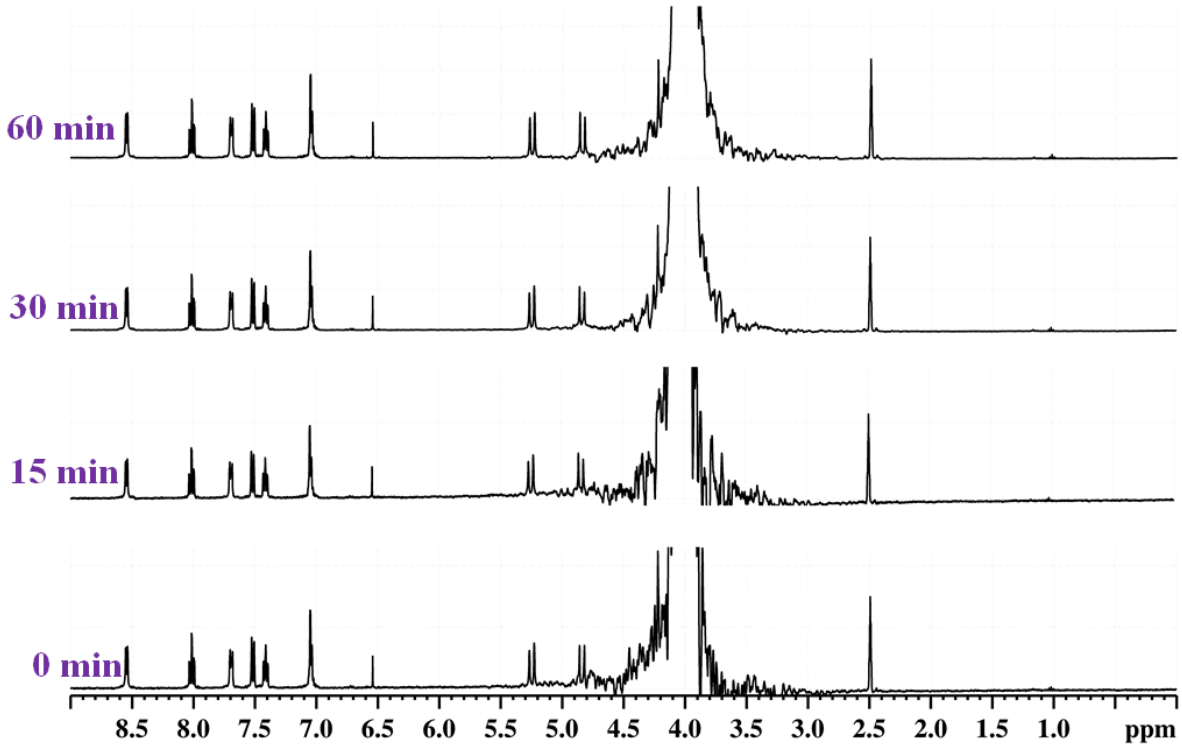

Figure S37. Photostability studies of complex **1** by ^{1}H NMR in DMSO-d_6-DPBS mixture (dose: 10 J/cm^2, 400-700 nm wavelength).

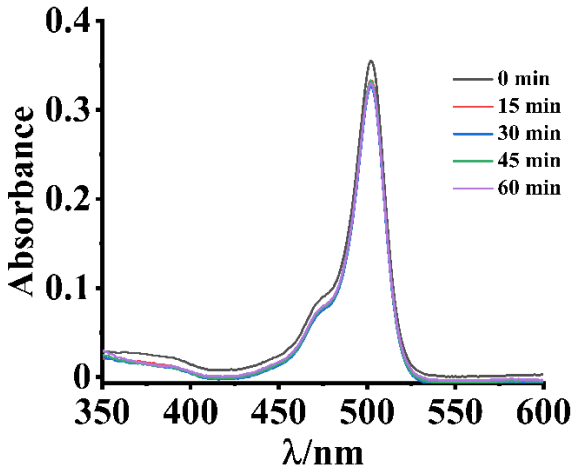

Figure S38. Photostability studies of complex **2** in 10 % DMSO/DPBS (dose: 10 J/cm^2, 400-700 nm wavelength).

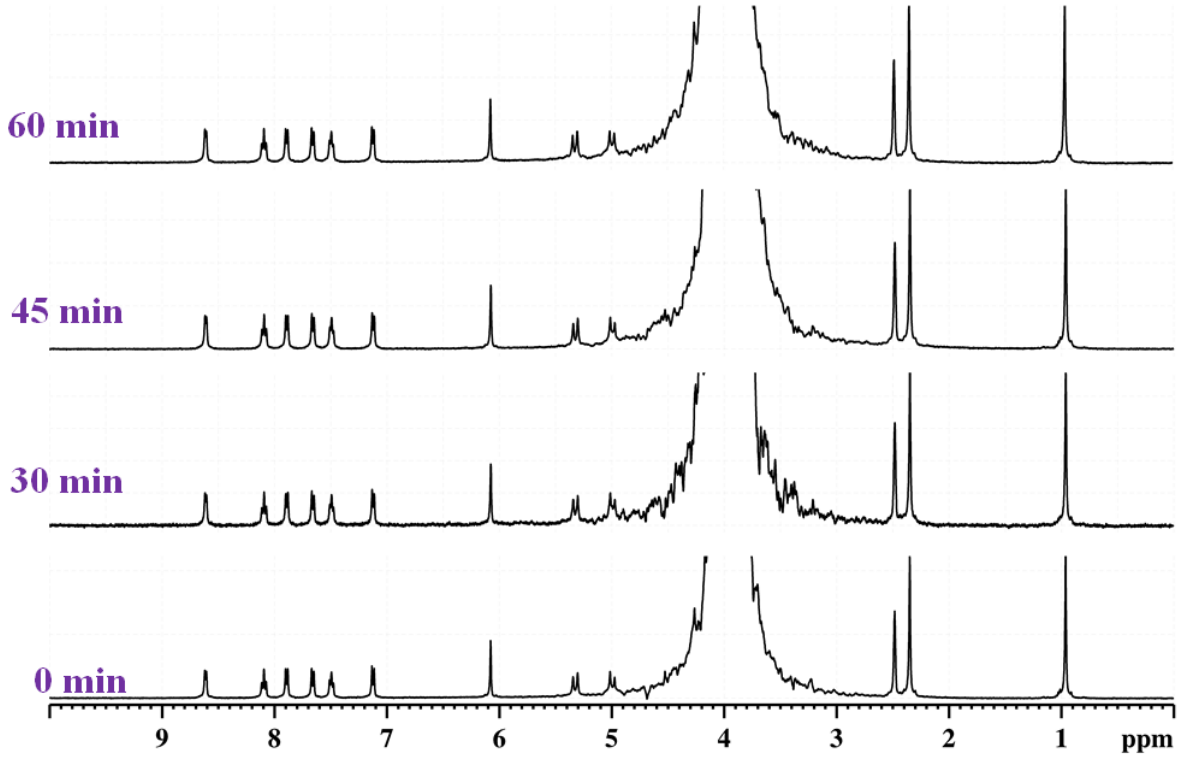

Figure S39. Photostability studies of complex **2** by ^{1}H NMR in DMSO-d_6-DPBS mixture (dose: 10 J/cm^2, 400-700 nm wavelength).

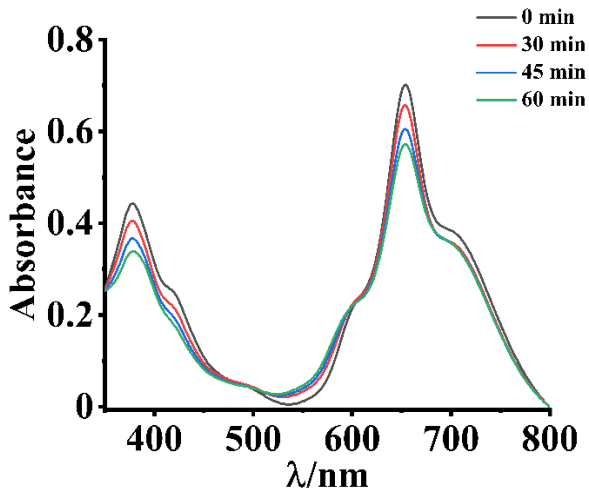

Figure S40. Photostability studies of complex **3** in 10 % DMSO/DPBS (dose: 30 J/cm^2, 600-720 nm wavelength).

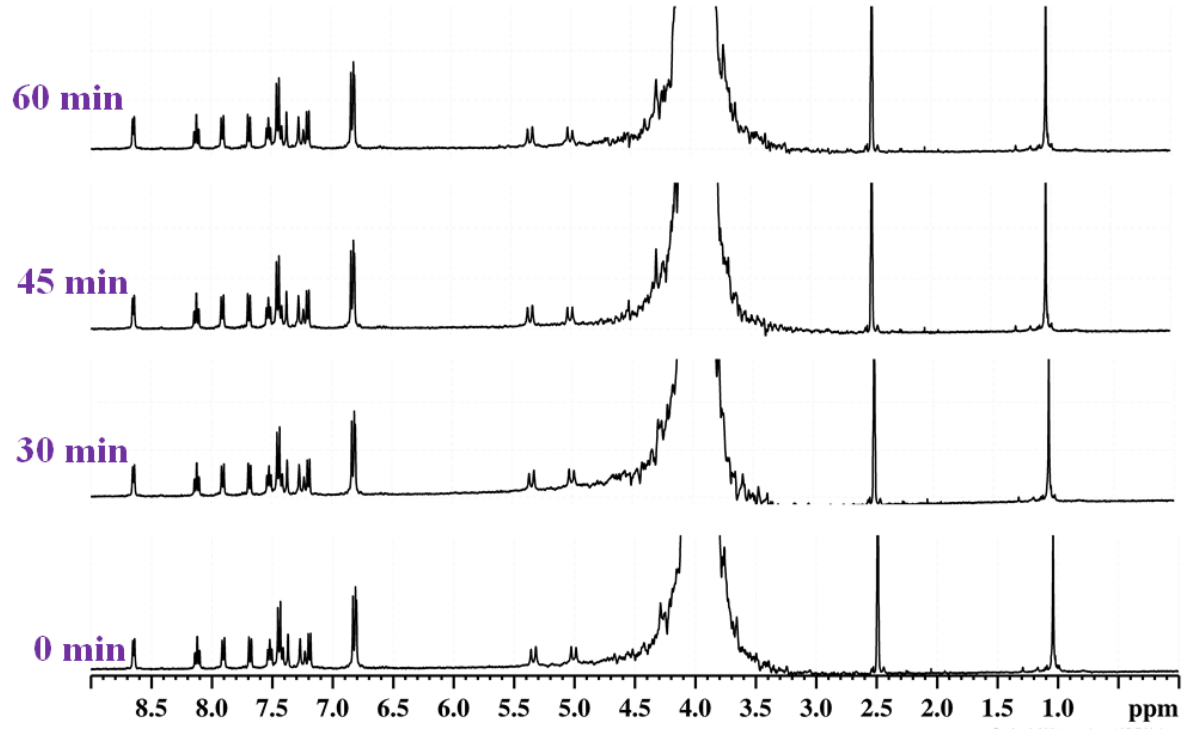

Figure S41. Photostability studies of complex **3** by ^{1}H NMR in DMSO-d_6-DPBS mixture (dose: 30 J/cm^2, 600-720 nm wavelength).

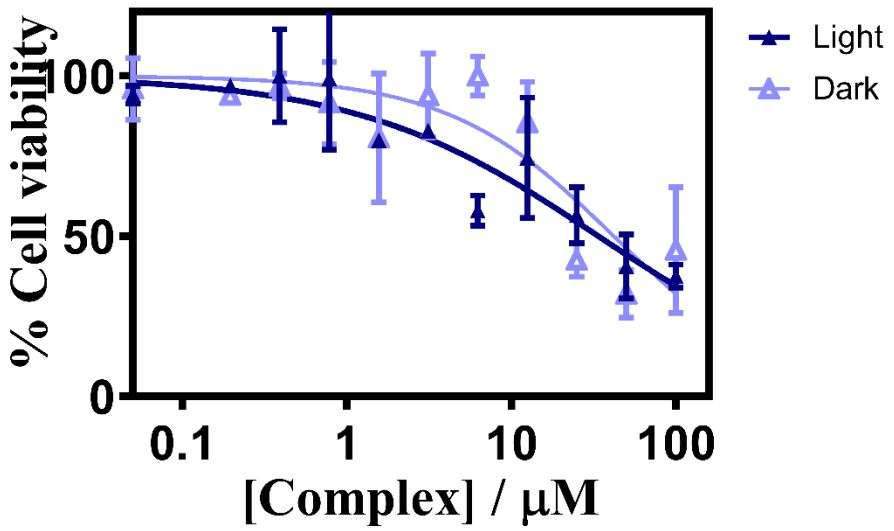

Figure S42. Cell viability plots obtained from MTT assay of complex **1** in HeLa cells under light (400-700 nm, 1 h exposure, light dose: 10 J cm^{-2}) and dark condition.

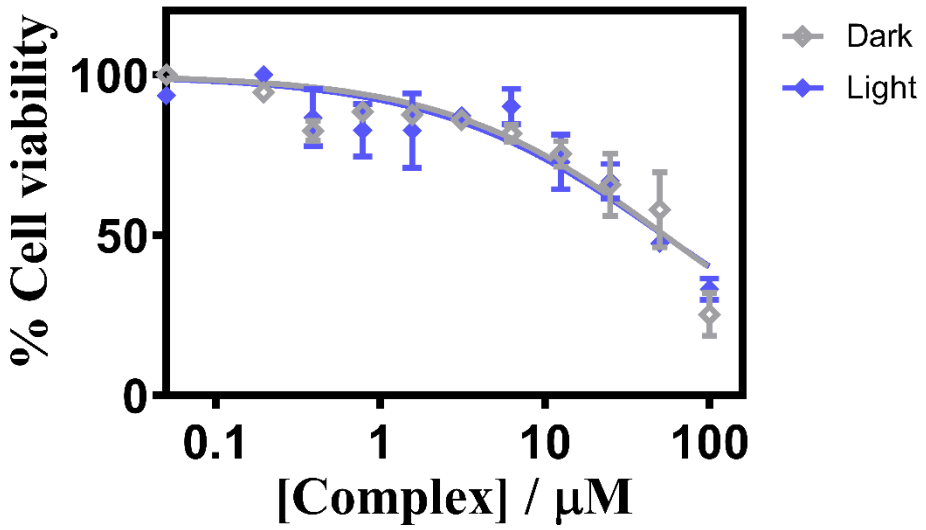

Figure S43. Cell viability plots obtained from MTT assay of complex **1** in A549 cell line under light (400-700 nm, 1 h exposure, light dose: 10 J cm^{-2}) and dark condition.

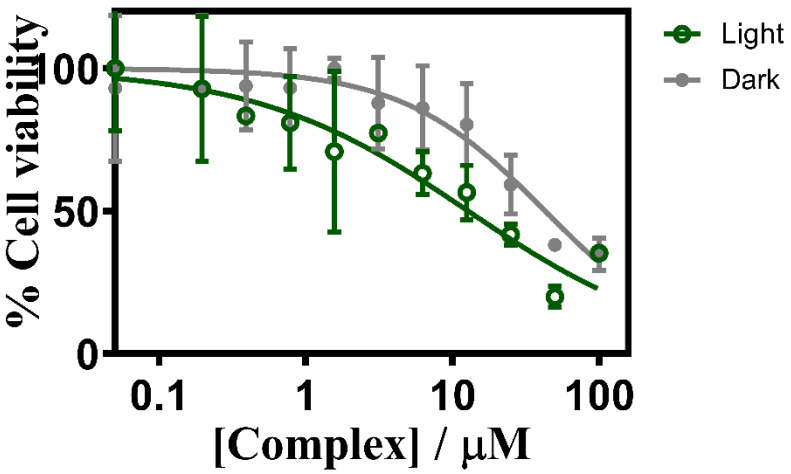

Figure S44. Cell viability plots obtained from MTT assay of complex **2** in HeLa cell line under light (400-700 nm, 1 h exposure, light dose: 10 J cm^{-2}) and dark condition.

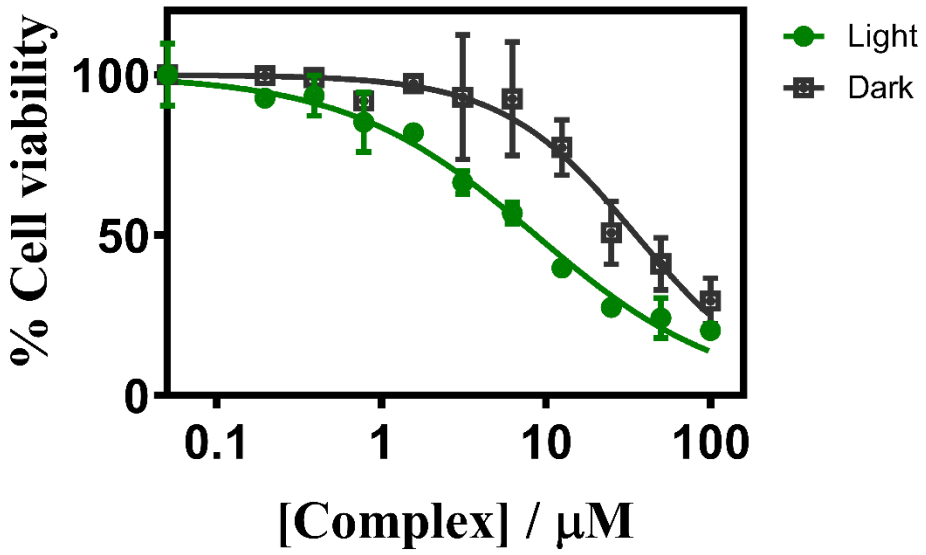

Figure S45. Cell viability plots obtained from MTT assay of complex **2** in A549 cell line under light (400-700 nm, 1 h exposure, light dose: 10 J cm^{-2}) and dark condition.

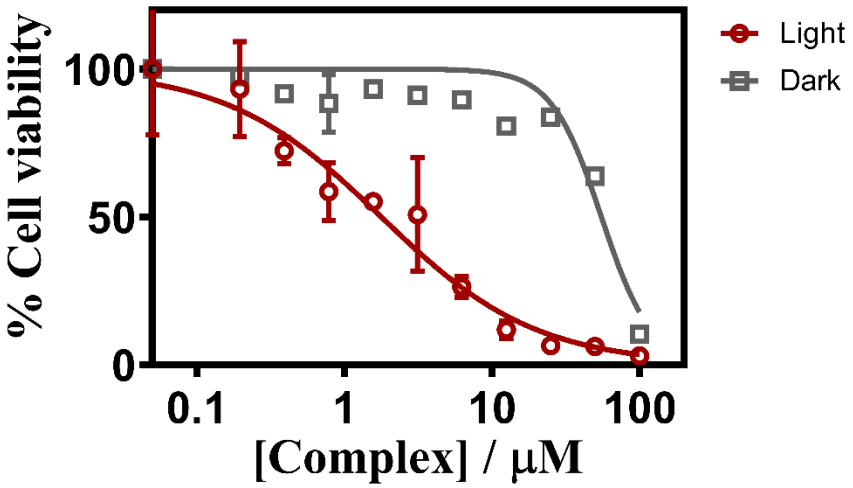

Figure S46. Cell viability plots obtained from MTT assay of complex **3** in HeLa cell line under light (600-720 nm, 20 min exposure, light dose: 30 J cm^{-2}) and dark condition.

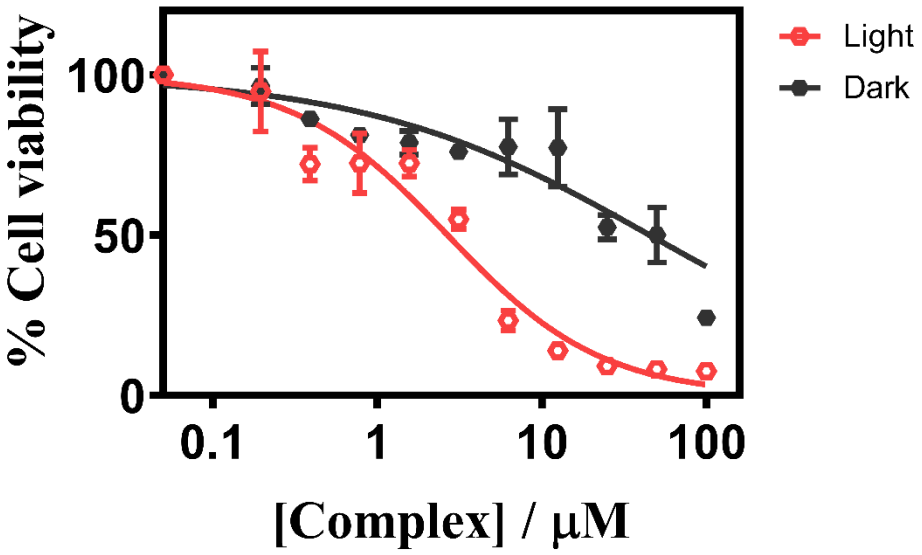

Figure S47. Cell viability plots obtained from MTT assay of complex **3** in A549 cell line under light (600-720 nm, 20 min exposure, light dose: 30 J cm^{-2}) and dark condition.

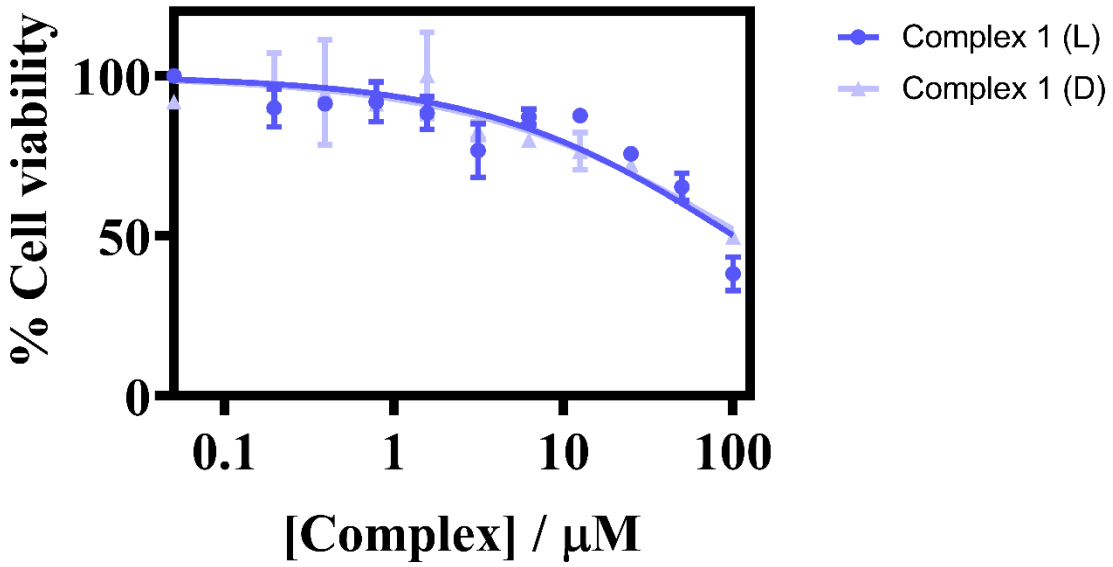

Figure S48. Cell viability plots obtained from MTT assay of complex **1** in HPL1D cells under light (400-700 nm, 1 h exposure, light dose: 10 J cm^{-2}) and dark condition.

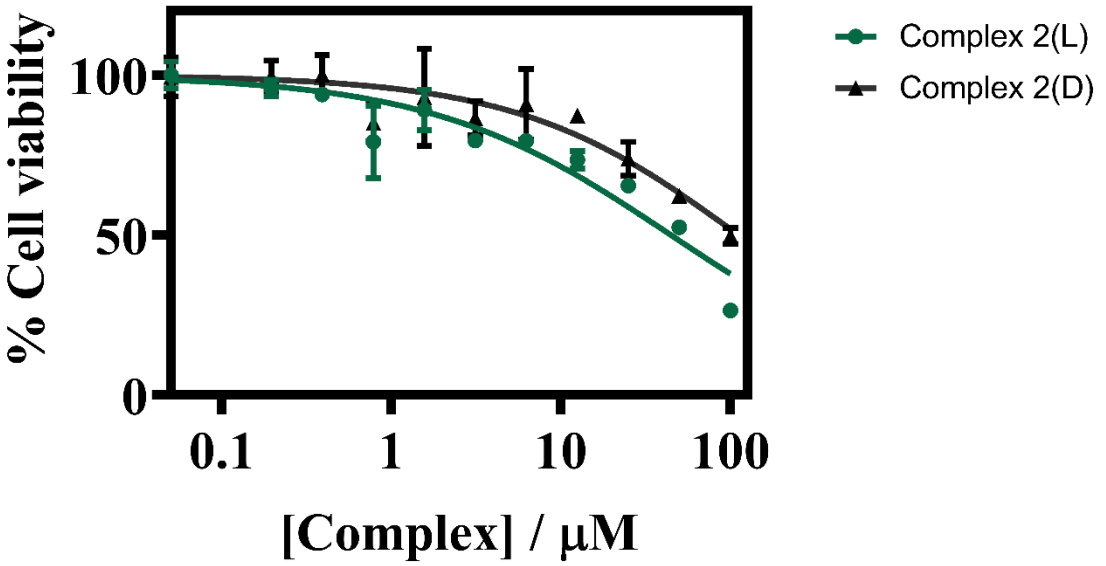

Figure S49. Cell viability plots obtained from MTT assay of complex **2** in HPL1D cells under light (400-700 nm, 1 h exposure, light dose: 10 J cm^{-2}) and dark condition.

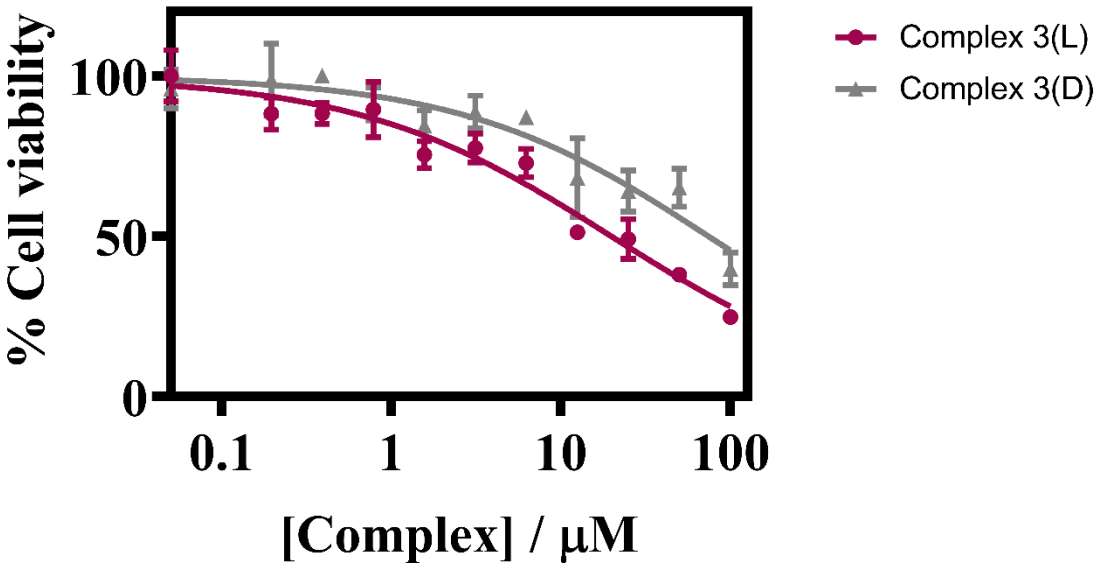

Figure S50. Cell viability plots obtained from MTT assay of complex **3** in HPL1D cells under light (600-720 nm, 20 min exposure, light dose: 30 J cm^{-2}) and dark condition.

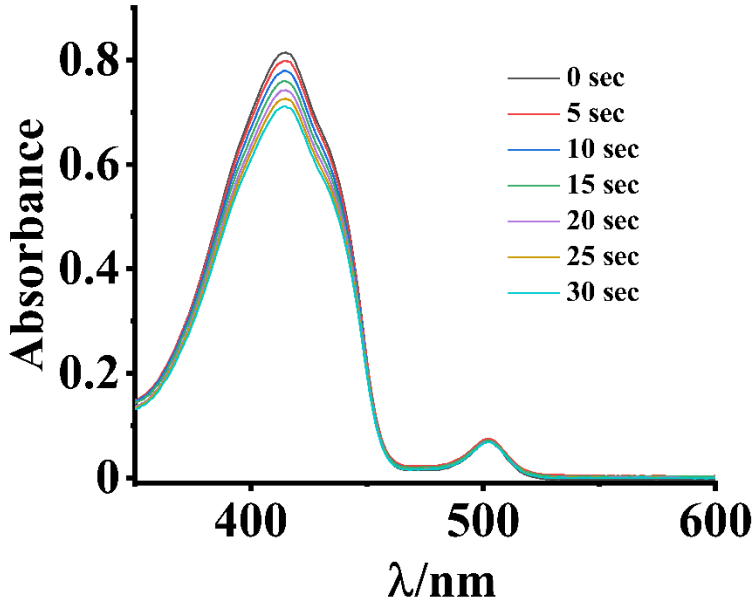

Figure S51. Changes in absorption spectra of DBBF containing complex **2** (50:1 concentration ratio) under visible light (400-700 nm, 10 J cm^{-2}) in DMSO.

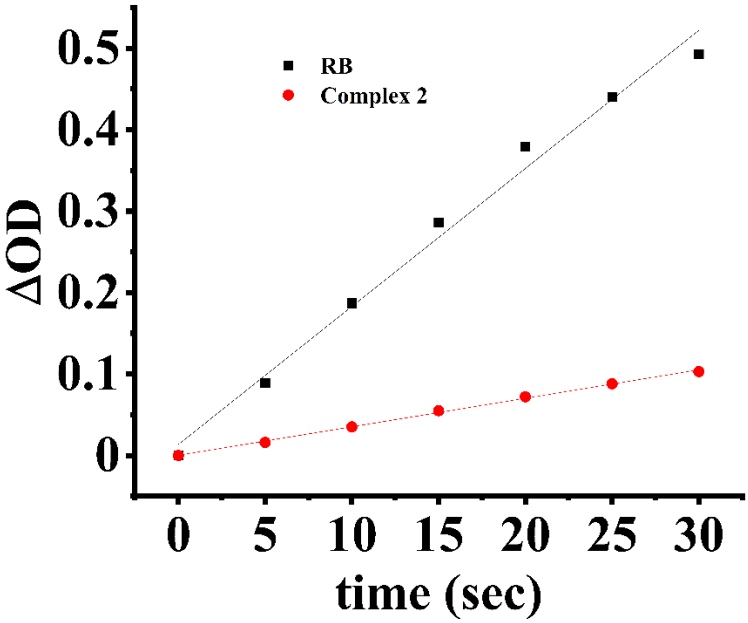

Figure S52. ΔOD vs. irradiation time for determining singlet oxygen quantum yield of complex **2**.

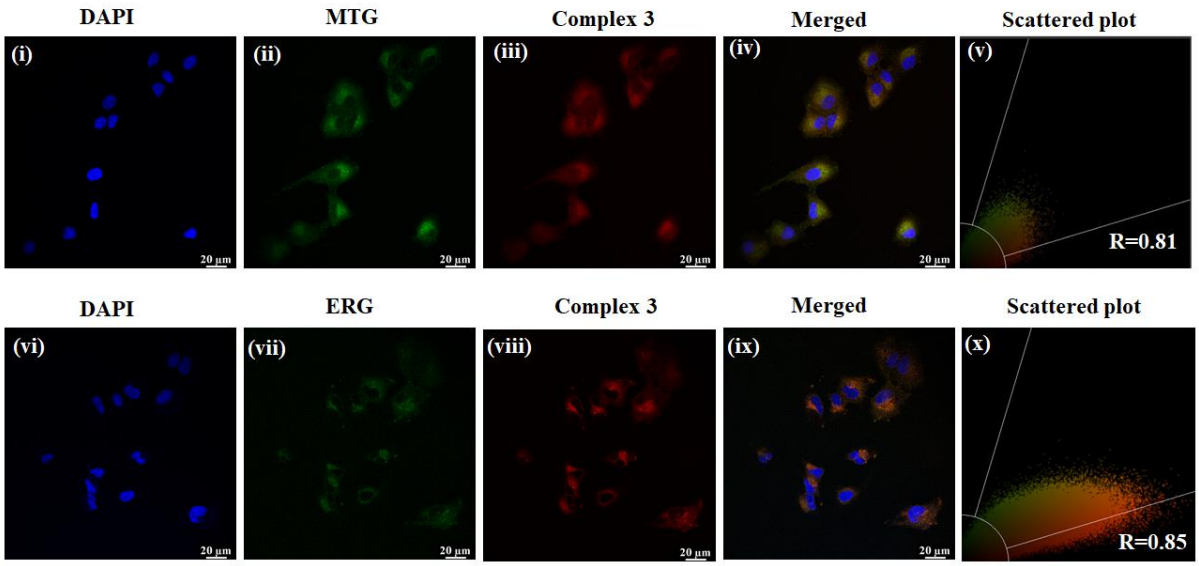

Figure S53. Confocal images for A549 cells with suitable trackers and complex **3**. Panels (i) and (vi) show blue emission of nucleus staining dye DAPI, panels (ii) and (vii) show green emission of trackers (iii) and (viii) show red emission of complex 3, panels (iv) and (ix) show merged images and (v) and (x) show scattered plot for Pearson's correlation coefficient (R) calculations.

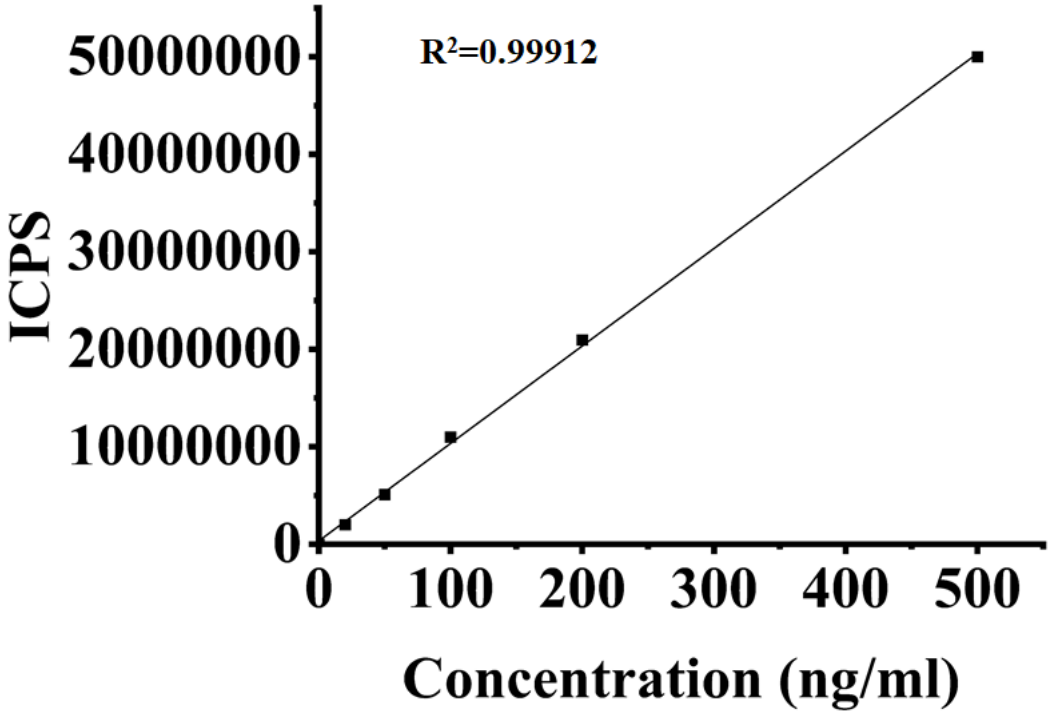

Figure S54. Standard plot for ICP-MS study for Pt content determination.

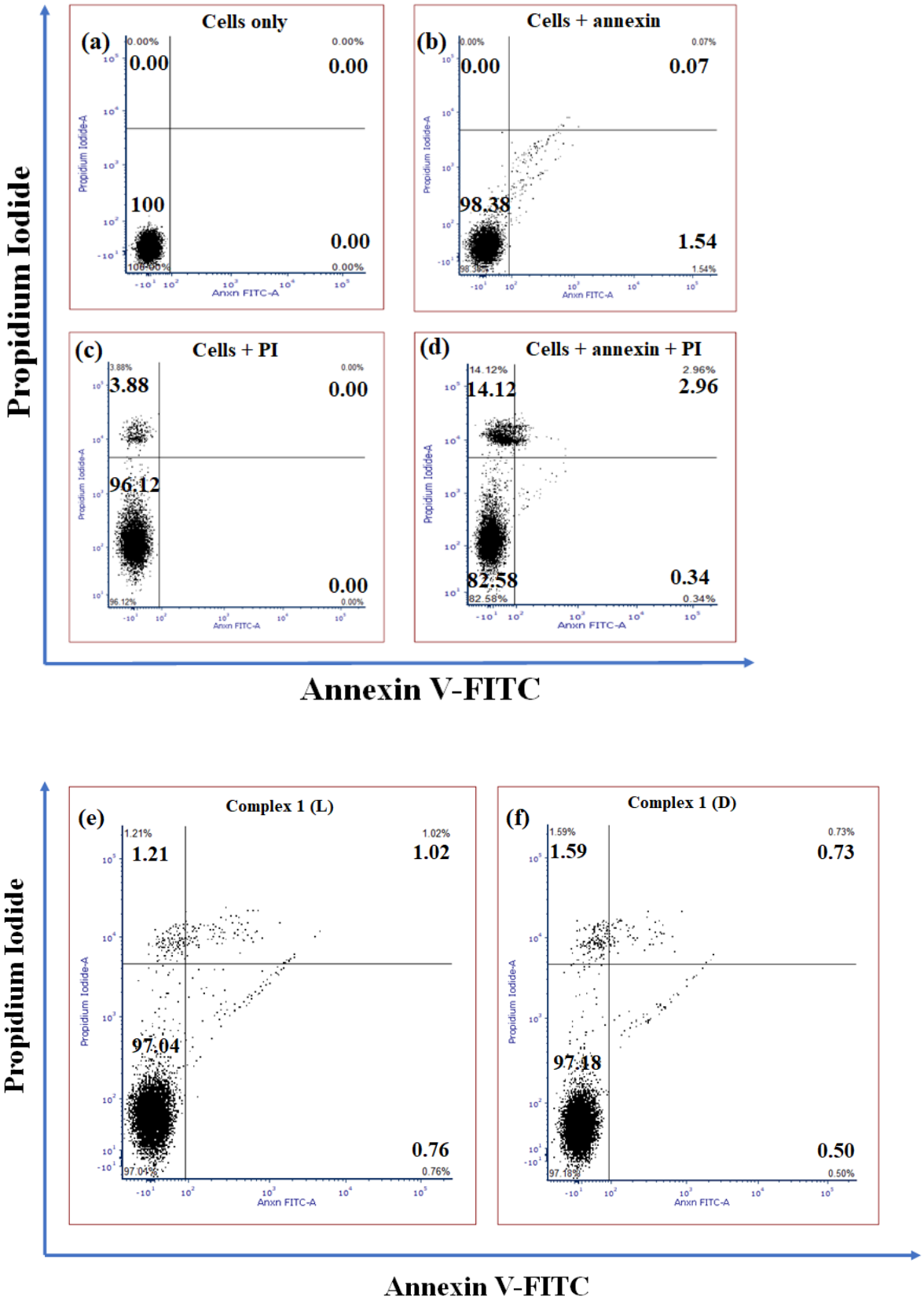

Figure S55. Dot plot of annexin V-FITC/PI data of (a) cells only, (b) cells + annexin, (c) cells + PI, (d) cells + annexin +PI, (e) cells + complex **1** (in light, λ =600-720 nm, 30 J cm^{-2}, 20 min irradiation) and (f) cells + complex **1** (in dark) in A549 cell line.

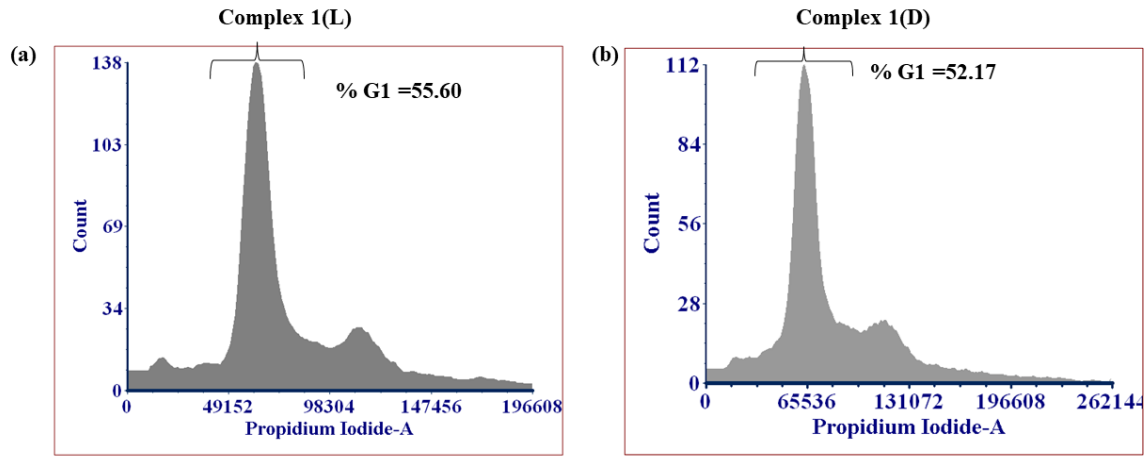

Figure S56. Cell cycle progression of complex **1** under (a) light and (b) dark condition using A549 cancer cell line.

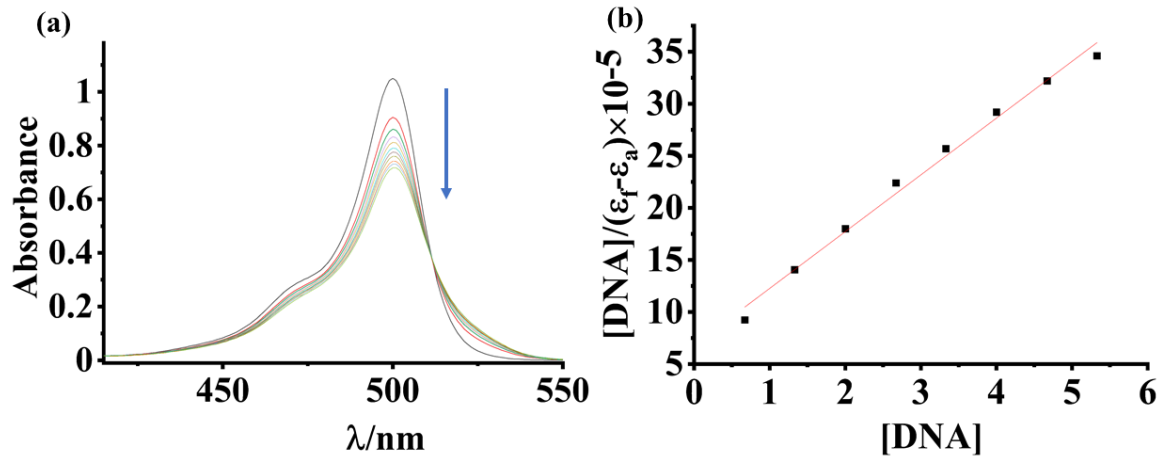

Figure S57. DNA binding plot for complex **2** in presence of 10 % DMF-Tris-HCl buffer (pH = 7.2) and ct-DNA at 25 °C. (a) changes in absorption spectra with each addition of ct-DNA and (b) McGhee-von Hippel (MvH) plot [DNA]/(ε_f - ε_a) vs. [DNA].

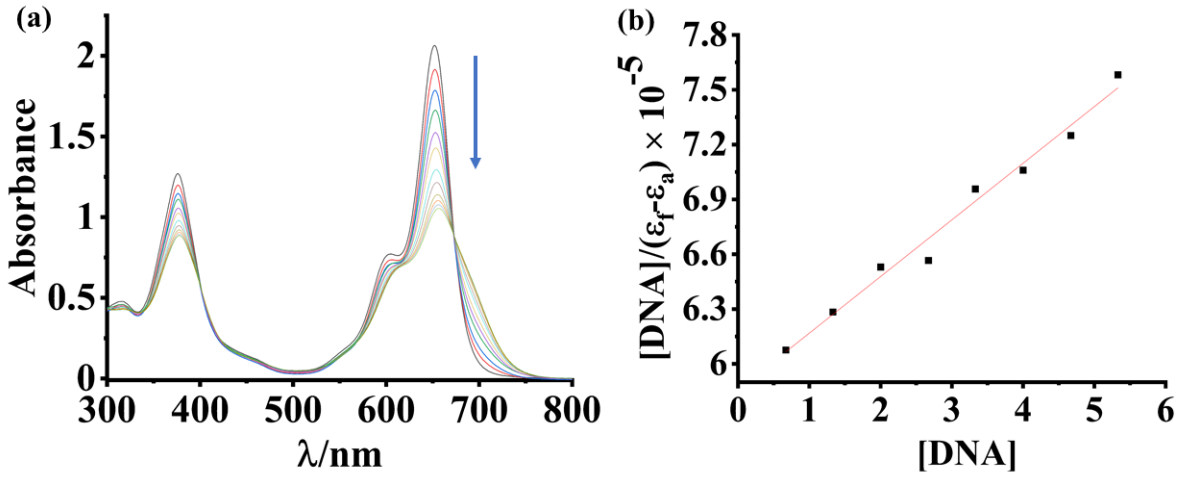

Figure S58. DNA binding plot for complex **3** in presence of 10 % DMF-Tris-HCl buffer (pH = 7.2) and ct-DNA at 25 °C. a) changes in absorption spectra with each addition of ct-DNA and (b) McGhee-von Hippel (MvH) plot [DNA]/(ε_f - ε_a) vs. [DNA].

Table S1. Selected crystallographic parameters for complex **2a**

formula	$C_{34}H_{32}BCl_2F_2N_6O_4Pt$
Formula weight	903.45
T/K	100
crystal system	monoclinic
Space group	P2/c
a/Å	19.1358(7)
b/Å	15.9715(7)
c/Å	24.4234(8)
α/°	90
β/°	109.955(2)
γ/°	90
Z	8
V/Å^3	7016.43(4)
μ(mm^{-1})	4.210
ρ_{cal}/g cm^{-3}	1.711
R[a] (I > 2σ (I))	0.0436
R (all data)	0.0692
wR[b] (I > 2σ (I))	0.115
wR (all data)	0.130

[a] $R = \Sigma||F_o| - |F_c||/\Sigma|F_o|$. [b] $wR = \Sigma[w(F_o^2 - F_c^2)^2]/\Sigma[w(F_o)^2]\}^{1/2}$.
[b] $w = 1/[\sigma^2 (F_o^2) + (aP)^2 + bP]$, where a=0.0541, b=31.16 and $P = (F_o^2 + 2F_c^2)/3$.

Table S2. Selected bonding parameters, namely, bond lengths (Å) and bond angles (°) for complex **2a**

Bond lengths	Pt(1A)-Cl(1A)	2.289(1)
	Pt(1B)-Cl(2B)	2.296(2)
	Pt(1A)-N(1A)	2.010(4)
	Pt(1B)-N(1B)	1.997(4)
	Pt(1A)-N(2A)	2.032(4)
	Pt(1B)-N(2B)	2.032(4)
	Pt(1A)-N(3A)	2.004(4)
	Pt(1B)-N(3B)	2.001(4)
Bond angles	N(2A)-Pt(1A)-Cl(1A)	178.0(1)
	N(2B)-Pt(1B)-Cl(2B)	178.8(1)
	N(1A)-Pt(1A)-N(3A)	167.1(2)
	N(1B)-Pt(1B)-N(3B)	166.6(2)

	N(2A)-Pt(1A)-N(3A)	85.0(1)
	N(2B)-Pt(1B)-N(3B)	84.6(2)
	N(1A)-Pt(1A)-N(2A)	83.6(2)
	N(1B)-Pt(1B)-N(2B)	83.3(2)

Table S3. Coordinates of optimized geometry for complex **1** obtained from DFT using B3LYP/LanL2DZ level of theory for all atoms.

Pt	-3.512133000	0.355958000	-0.435253000
Cl	-4.023891000	1.150511000	-2.643080000
N	-4.722525000	-1.275724000	-0.517162000
N	-3.089136000	-0.345483000	1.484334000
N	-2.330666000	1.918693000	0.096202000
C	-5.251574000	-1.851950000	-1.628444000
C	-6.057108000	-2.996540000	-1.533319000
C	-6.309831000	-3.555766000	-0.269156000
C	-5.753268000	-2.951011000	0.876972000
C	-4.967029000	-1.805361000	0.730007000
C	-4.394572000	-1.018324000	1.900170000
C	-2.759317000	0.896764000	2.298046000
C	-2.056239000	1.941911000	1.443148000
C	-1.231895000	2.932445000	1.984637000
C	-0.688263000	3.916993000	1.136873000
C	-0.982522000	3.879939000	-0.237103000
C	-1.807063000	2.860966000	-0.732307000
C	-1.959926000	-1.401789000	1.560055000
C	-0.565523000	-0.915359000	1.227283000
C	0.355550000	-0.663340000	2.268493000
C	1.673418000	-0.263354000	1.979437000
C	2.085396000	-0.119179000	0.641072000
C	1.177258000	-0.383551000	-0.404222000
C	-0.138020000	-0.783215000	-0.113165000
H	-2.265865000	-2.203919000	0.881536000
H	-1.982711000	-1.791347000	2.587843000

H	-5.935504000	-3.363208000	1.864423000
H	-6.926317000	-4.444210000	-0.172814000
H	-6.471200000	-3.431666000	-2.436095000
H	-5.023639000	-1.367801000	-2.570824000
H	-4.240110000	-1.665020000	2.772679000
H	-5.102027000	-0.227738000	2.175519000
H	-2.150045000	0.637640000	3.170614000
H	-3.706945000	1.316322000	2.657039000
H	-1.015484000	2.936415000	3.048174000
H	-0.047337000	4.693774000	1.542572000
H	-0.584024000	4.621403000	-0.920631000
H	-2.074630000	2.776700000	-1.778985000
H	0.056894000	-0.806065000	3.306410000
H	-0.827305000	-0.997990000	-0.927069000
H	2.376313000	-0.083819000	2.788452000
H	1.497968000	-0.292949000	-1.438452000
H	3.105721000	0.178327000	0.414131000

Table S4. Coordinates of optimized geometry for complex **2** obtained from DFT using B3LYP/LanL2DZ level of theory for all atoms.

Pt	-3.465669000	0.395131000	-0.438406000
Cl	-3.948343000	1.144368000	-2.667651000
F	7.144739000	-0.158162000	-1.784575000
F	7.655517000	-0.092397000	0.495145000
N	-4.641137000	-1.262182000	-0.527440000
N	-3.069524000	-0.280536000	1.495525000
N	-2.368678000	2.011118000	0.112470000
N	5.792947000	-1.492548000	-0.244133000
N	5.601614000	0.987699000	-0.274409000
C	-5.131469000	-1.868425000	-1.640345000
C	-5.930907000	-3.017168000	-1.542284000
C	-6.218746000	-3.548192000	-0.273512000
C	-5.702087000	-2.912407000	0.874709000

C	-4.919923000	-1.764587000	0.724154000
C	-4.387788000	-0.944849000	1.890958000
C	-2.744455000	0.957373000	2.316590000
C	-2.120193000	2.053318000	1.463415000
C	-1.402507000	3.115606000	2.022635000
C	-0.944711000	4.153798000	1.189384000
C	-1.208991000	4.094980000	-0.190015000
C	-1.921536000	3.003848000	-0.703381000
C	-1.959428000	-1.349190000	1.600322000
C	-0.549023000	-0.941414000	1.224525000
C	0.422640000	-0.770826000	2.235160000
C	1.774654000	-0.562144000	1.908751000
C	2.187914000	-0.528252000	0.561127000
C	1.213570000	-0.666620000	-0.452011000
C	-0.135749000	-0.876204000	-0.125669000
C	3.643485000	-0.406108000	0.214719000
C	4.413410000	-1.579785000	0.073889000
C	4.087230000	-2.986340000	0.192697000
C	2.767927000	-3.640765000	0.513363000
C	5.273923000	-3.687551000	-0.057028000
C	6.313314000	-2.750577000	-0.323599000
C	7.749389000	-3.026652000	-0.640654000
C	5.922481000	2.308981000	-0.389443000
C	7.301159000	2.792591000	-0.713237000
C	4.749685000	3.079358000	-0.149650000
C	3.686291000	2.205683000	0.119317000
C	2.276688000	2.644198000	0.417880000
C	4.225855000	0.868846000	0.041327000
B	6.574890000	-0.187271000	-0.458106000
H	-2.293677000	-2.174797000	0.964311000
H	-1.974856000	-1.695225000	2.643689000
H	2.889556000	-4.728916000	0.533583000
H	1.999301000	-3.404330000	-0.232669000
H	2.379374000	-3.329254000	1.490655000

H	7.932216000	-4.103865000	-0.683021000
H	8.028627000	-2.574605000	-1.599871000
H	8.405943000	-2.580422000	0.116560000
H	8.016257000	2.461205000	0.049682000
H	7.646177000	2.373128000	-1.665921000
H	7.320762000	3.884358000	-0.772782000
H	1.942970000	2.312868000	1.409379000
H	1.560133000	2.250345000	-0.313878000
H	2.218196000	3.738018000	0.390354000
H	-5.912257000	-3.302049000	1.865758000
H	-6.832434000	-4.438330000	-0.175070000
H	-6.314419000	-3.476615000	-2.446519000
H	-4.880119000	-1.404190000	-2.586748000
H	-4.258418000	-1.567144000	2.785249000
H	-5.103559000	-0.147715000	2.121144000
H	-2.083914000	0.698896000	3.151364000
H	-3.684161000	1.335924000	2.737068000
H	-1.209976000	3.137485000	3.090806000
H	-0.394173000	4.989255000	1.610586000
H	-0.875052000	4.876055000	-0.863879000
H	-2.166219000	2.902566000	-1.754120000
H	0.138590000	-0.846377000	3.284064000
H	-0.862529000	-1.012654000	-0.923572000
H	2.513952000	-0.460027000	2.698423000
H	1.519912000	-0.642404000	-1.494192000
H	4.704612000	4.159285000	-0.175553000
H	5.397276000	-4.761529000	-0.052376000

Table S5. Coordinates of optimized geometry for complex **3** obtained from DFT using B3LYP/LanL2DZ level of theory for all atoms.

Pt	-5.857010000	0.337202000	-0.580262000
Cl	-6.207748000	1.146503000	-2.813562000
F	4.900421000	-0.118137000	-1.069747000
F	5.182934000	-0.100422000	1.235448000

O	11.327712000	-5.782955000	-0.707658000
O	10.324269000	6.490736000	-0.760464000
N	-7.014280000	-1.321674000	-0.788713000
N	-5.579027000	-0.390738000	1.354444000
N	-4.803955000	1.940316000	0.082733000
N	3.400675000	-1.495174000	0.294463000
N	3.196738000	0.987417000	0.302116000
C	-7.428425000	-1.898522000	-1.947174000
C	-8.225053000	-3.053232000	-1.932538000
C	-8.589975000	-3.620894000	-0.699919000
C	-8.151205000	-3.015609000	0.496188000
C	-7.368300000	-1.860438000	0.427993000
C	-6.914989000	-1.071522000	1.648049000
C	-5.313709000	0.825067000	2.228179000
C	-4.639192000	1.944286000	1.447039000
C	-3.958437000	2.989779000	2.079139000
C	-3.451198000	4.050560000	1.305360000
C	-3.629993000	4.030913000	-0.088731000
C	-4.308333000	2.955288000	-0.675682000
C	-4.469633000	-1.457192000	1.499337000
C	-3.039753000	-1.024266000	1.249811000
C	-2.153677000	-0.878150000	2.340144000
C	-0.782837000	-0.645983000	2.129567000
C	-0.261466000	-0.564344000	0.821448000
C	-1.152676000	-0.675586000	-0.269444000
C	-2.521550000	-0.908043000	-0.060217000
C	1.215994000	-0.426634000	0.597452000
C	2.005484000	-1.592669000	0.492623000
C	1.672809000	-3.004447000	0.549799000
C	0.329964000	-3.662732000	0.741765000
C	2.867671000	-3.702058000	0.386449000
C	3.938289000	-2.761574000	0.229090000
C	3.520107000	2.325528000	0.242369000
C	2.310757000	3.075900000	0.405983000

C	1.248314000	2.186685000	0.566716000
C	-0.186644000	2.600998000	0.762746000
C	1.806574000	0.853718000	0.501671000
C	5.345676000	-3.006196000	0.036201000
C	4.869545000	2.795540000	0.047109000
C	5.894791000	-4.260024000	-0.007979000
C	5.209555000	4.120194000	-0.010862000
C	7.304956000	-4.590013000	-0.195323000
C	7.697422000	-5.956816000	-0.198424000
C	8.318321000	-3.610226000	-0.374779000
C	9.031605000	-6.338330000	-0.368779000
C	9.656946000	-3.978467000	-0.546707000
C	10.015159000	-5.345526000	-0.543030000
C	6.548616000	4.671034000	-0.205591000
C	6.713652000	6.082779000	-0.242511000
C	7.708543000	3.865566000	-0.362360000
C	7.968064000	6.672380000	-0.426595000
C	8.969617000	4.442683000	-0.547231000
C	9.100384000	5.849299000	-0.579833000
B	4.183866000	-0.181114000	0.188509000
H	-4.747740000	-2.258636000	0.807830000
H	-4.560937000	-1.844097000	2.524368000
H	0.448221000	-4.751736000	0.739962000
H	-0.375070000	-3.402418000	-0.057105000
H	-0.136147000	-3.378901000	1.693019000
H	-0.592117000	2.243019000	1.717587000
H	-0.838469000	2.216108000	-0.031433000
H	-0.257906000	3.694701000	0.755060000
H	-8.421202000	-3.434163000	1.460579000
H	-9.203190000	-4.516145000	-0.665676000
H	-8.546870000	-3.488910000	-2.871926000
H	-7.119386000	-1.406360000	-2.861862000
H	-6.837503000	-1.718205000	2.530923000
H	-7.649014000	-0.284684000	1.855329000

H	-4.708172000	0.545599000	3.097142000
H	-6.280745000	1.190328000	2.595117000
H	-3.830822000	2.980405000	3.157128000
H	-2.927459000	4.872731000	1.783037000
H	-3.254854000	4.829866000	-0.718501000
H	-4.486367000	2.883986000	-1.742145000
H	-2.519899000	-0.992747000	3.359830000
H	-3.181330000	-1.022928000	-0.917862000
H	-0.108994000	-0.564830000	2.978031000
H	-0.763434000	-0.614201000	-1.282015000
H	2.237968000	4.154236000	0.403519000
H	2.972231000	-4.777563000	0.377480000
H	5.973870000	-2.129044000	-0.073682000
H	5.630352000	2.029656000	-0.056132000
H	5.234033000	-5.119953000	0.110118000
H	4.418686000	4.864199000	0.095846000
H	6.940007000	-6.726569000	-0.063438000
H	8.061184000	-2.555081000	-0.380642000
H	9.332110000	-7.381036000	-0.370407000
H	10.419693000	-3.213245000	-0.682884000
H	5.840747000	6.722122000	-0.124880000
H	7.627396000	2.782776000	-0.340107000
H	8.094563000	7.749771000	-0.455046000
H	9.846995000	3.808566000	-0.665574000
H	11.961600000	-5.045464000	-0.822566000
H	11.069462000	5.863681000	-0.862334000

Table S6. Comparison of IC_{50} (μM) values of complexes **1-3** with recently reported platinum(II)-anticancer complexes

Entry	HeLa		A549	
	Dark	Light	Dark	Light
Complex **1**[a]	41.9 ± 3.1	33.8 ± 2.1	53.3 ± 2.6	52.8 ± 3.2
Complex **2**[a]	42.9 ± 2.5	12.8 ± 1.6	35.3 ± 2.1	10.0 ± 1.1

Complex **3**[b]	55.1 ± 2.9	1.8 ± 0.6	45.3 ± 1.3	2.7 ± 0.2
Pt^{II}-(cyclometallating ligand) conjugate[c]	1.6	0.2		
Pt(BDPA)[d]	>50	4.7±2.1	>50	3.8±0.5
Pt^{II}-(pyridyl-diiodo-BODIPY) conjugate[e]	n.d.	n.d.	73.2±1.1	0.05±0.01
Binuclear Pt^{II}-BODIPY conjugate[f]	105.0±3.2	0.6±0.2	96.4±0.8	0.7±0.2
Maloplatin-B[g]	79.0±3.2	2.4±0.2	85.0±0.4	1.6±0.2
Pt^{II}-(curcumin-Biotin conjugate)[h]	57.0±0.2	8.5±0.3	62.8±1.5	9.8±0.3

[a]Used in this study. Light source: Luzchem photoreactor, λ=400-700 nm, dose: 10 J cm^{-2}, irradiation time: 1 h. [b] used in this study. Waldmann PDT photoreactor, λ=600-720 nm, dose: 30 J cm^{-2}, irradiation time: 20 min. [c]Data from reference S7, 405 nm wavelength, dose: 3.6 J cm^{-2}, irradiation time: 3 min. [d]Data from reference S8, 532 nm wavelength, power density: 3.5 mW cm^{-2}, irradiation time: 5 min. [e]Data from reference S9, Light source: Luzchem photoreactor, λ=400-700 nm, dose: 10 J cm^{-2}, irradiation time: 1 h. [f]Data from reference S10, Waldmann PDT photoreactor, λ=600-720 nm, dose: 30 J cm^{-2}, irradiation time: 15 min. [g]Data from reference S11, Waldmann PDT photoreactor, λ=600-720 nm, dose: 30 J cm^{-2}, irradiation time: 15 min. [h] Data from reference S12, Light source: Luzchem photoreactor, λ=400-700 nm, dose: 10 J cm^{-2}, irradiation time: 1 h. n.d. – not determined.

References-

S1. G. M. Sheldrick, *Acta Crystallogr., Sect. C: Struct. Chem.*, 2015, **C71**, 3-8.

S2. H. He, P-C. Lo, S-L. Yeung, W. P. Fong and D. K. P. Ng. *J. Med. Chem*., 2011, **54**, 3097-3102.

S3. L. J. Farrugia, *J. Appl. Crystallogr.*, 2012, **45**, 849-854.

S4. A. D. Becke, *Phys. Rev. A: At. Mol., Opt. Phys.*, 1988, **38**, 3098-3100.

S5. A. D. Becke, *J. Chem. Phys.*, 1993, **98**, 5648.

S6. M. J. Frisch, G. W. Trucks, H. B. Schlegel, G. E. Scuseria, M. A. Robb, J. R. Cheeseman, J. A., Jr. Montgomery, T. Vreven, K. N. Kudin, J. C. Burant, J. M. Millam, S. S. Iyengar, J. Tomasi, V. Barone, B. Mennucci, M. Cossi, G. Scalmani, N. Rega, G. A. Petersson, H. Nakatsuji, M. Hada, M. Ehara, K. Toyota, R. Fukuda, J. Hasegawa, M. Ishida, T. Nakajima, Y. Honda, O. B. Cross, V. Bakken, C. Adamo, J. Jaramillo, R. Gomperts, R. E. Stratmann, O. Yazyev, A. J. Austin, R. Cammi, C. Pomelli, J. W. Ochterski, P. Y. Ayala, K. Morokuma, G. A. Voth, P. Salvador, J. J. Dannenberg, V. G. Zakrzewski, S. Dapprich, A. D. Daniels, M. C. Strain, O. Farkas, D. K. Malick, A. D. Rabuck, K. Raghavachari, J. B. Foresman, J. V. Ortiz, Q. Cui, A. G. Baboul, S. Clifford, J. Cioslowski, B. B. Stefanov, G. Liu, A. Liashenko, P. Piskorz, I. Komaromi, R. L. Martin, D. J. Fox, T. Keith, M. A. Al-Laham, C. Y. Peng, A. Nanayakkara, M. Challacombe, P. M. W. Gill, B. Johnson, W. Chen, M. W. Wong, C. Gonzalez, and J. A. Pople, *Gaussian 03*, revision B.4; Gaussian Inc.: Pittsburgh, PA, 2003.

S7. R. E. Doherty, I. V. Sazanovich, L. K. McKenzie, A. S. Stasheuski, R. Coyle, E. Baggaley, S. Bottomley, J. A. Weinstein and H. E. Bryant, *Sci. Rep.*, 2016, **6**, 22668.

S8. X. Xue, C. Qian, H. Fang, H. K. Liu, H. Yuan, Z. Guo, Y. Bai and W. He, *Angew. Chem., Int. Ed.*, 2019, **58**, 12661-12666.

S9. M. K. Raza, S. Gautam, P. Howlader, A. Bhattacharyya, P. Kondaiah and A. R. Chakravarty, *Inorg. Chem.*, 2018, **57**, 14374-14385.

S10. V. Ramu, S. Gautam, P. Kondaiah and A. R. Chakravarty, *Inorg. Chem.*, 2019, **58**, 9067-9075.

S11. V. Ramu, P. Kundu, P. Kondaiah and A. R. Chakravarty, *Inorg. Chem.*, 2021, **60**, 6410-6420.

S12. A. Upadhyay, S. Gautam, V. Ramu, P. Kondaiah and A. R. Chakravarty, *Dalton Trans.*, 2019, **48**, 17556-17565.